Evaluation of GHBMC, THUMS and SAFER Human Body Models in Frontal Impacts in Reclined Postures

Bronislaw D. Gepner, Daniel Perez-Rapela, Jason L. Forman, Martin Ostling, Bengt Pipkorn, Jason R. Kerrigan

Abstract Virtual tools, such as human body models (HBMs), can support advances in vehicle development and restraint system design. The goal of this study is to evaluate selected HBMs against data from recent reclined post-mortem human subject (PMHS) tests. Three HBMs - the Global Human Body Modelling Consortium detailed model v.6.0, Total Human Model for Safety v.6.0, and SAFER HBM v.10 - were used in this study. The models were positioned with respect to the average PMHS position and utlised a previously developed environment model. The HBMs were evaluated comparing belt engagement, boundary forces and displacements (in the seat and belt), and the trajectories of the head, T1, T8, T11, L1, L3, and pelvis. The HBMs' belt engagement, boundary forces and displacements, and X-direction (fore-aft) trajectories were all generally consistent with the PMHS. All HBMs predicted more downward motion of the head and T1 compared to the PMHS. The HBMs also showed rearward pelvis pitch at peak lap belt force, opposite to the PMHS. Some of these differences were associated with differences in flexion of the lumbar spine. This is the first study to provide an in-depth evaluation of multiple reclined HBMs in frontal crashes compared to reclined PMHS.

Keywords: HBM, restraint, PMHS, recline, submarining

I. INTRODUCTION

With the introduction of Level 3 Autonomous Driving Systems (ADS) occupants may be given an opportunity to use new seating arrangements, which differ to the ones available in current vehicles. ADS Level 3 will enable drivers to disengage from vehicle controls for extended periods of time, allowing for other activities within the passenger compartment [1-3]. Some occupants may want a living room style interior arrangement, where occupants can face each other. Others might use the time when the vehicle takes over control to rest and relax [4-5]. This need may be addressed by forward facing reclined seating arrangement, where the occupant might be moved away from the instrument panel for increased comfort.

While introduction of advanced levels of vehicle autonomy is expected to improve safety, mainly by eliminating contribution of the human error, these vehicles are still expected to crash [6-7]. Automated driving systems may still be prone to occupant misuse (where autonomous mode is engaged outside of its area of applicability [8]), and will continue to face potential collision exposure in a mixed fleet environment where ADS vehicles share the road with manually driven cars. Thus, there will be a continuing need for future vehicle restraint systems to provide an appropriate level of occupant protection in the event of a collision. Considering the potential changes in vehicle interior configurations that may be enabled by the introduction of the ADS, there is a need for tools to evaluate restraint interactions and occupant protection in an expanded range of occupant postures and loading scenarios [9-11].

Traditionally, new restraint systems are developed using anthropomorphic test devices (ATDs), such as the Test devices for Human Occupant Restraint (THOR) or Hybrid-III. However, these ATDs are developed for, and only applicable to, specific loading conditions, e.g., frontal crashes with an upright occupant. There are ongoing efforts to evaluate the biofidelity of these ATDs in reclined scenarios, and to explore modifications to the THOR to expand its range of applicability. Given the challenges of physical surrogates, however, virtual tools such as human body models (HBMs) offer an attractive alternative. These models are developed using anthropometric and material data of the human body, and have the potential to serve as omni-directional dummies. However, they also depend on being validated in the scenarios in which they will be used.

B. D. Gepner is a Research Scientist (+1-434-297-8046 / bgepner@virginia.edu), D. Perez-Rapela was a Research Scientist, J. L. Forman is a Principal Scientist, J. R. Kerrigan is an Associate Professor of Mechanical and Aerospace Engineering at University of Virginia, USA., M. Östling is a Senior Specialist at Autoliv Research, Vårgårda, Sweden and B. Pipkorn is Adjunct Professor at Chalmers University of Technology and Director of Simulation and Active Structures at Autoliv Research.

To be useful as tools for evaluating occupant safety for future vehicle environments, HBMs must exhibit biofidelic responses when used with postures and restraint systems that are anticipated for such environments. Though validation data has thus far been limited, recent computational studies have elucidated the potential consequences of reclining on restraint interaction, informing the types of response characteristics that should be examined when considering model validation in such environments. In one-such simulation study with a reclined HBM, [9] found that a belt system with a B-pillar mounted D-ring resulted in late torso engagement, with increased pelvis excursion when compared with seatback integrated belts. Several other simulation studies have suggested that increased seatback recline may lead to increased risk of submarining, either with the passing over the iliac crest of the pelvis without engaging, or with the belt slipping over the pelvis after initial engagement [12-16]. The presence of knee restraints (knee bolster, knee airbag) was found to be an effective countermeasure for submarining in simulation [12-13] [17]. However, knee bolster restraint might not be available in future interiors when the occupant is moved away from the instrument panel. Belt-based countermeasures such as dual lap belt pretensioners have been shown to mitigate submarining risk in reclined simulations with some HBMs [18]. By elucidating the potential adverse consequences of (and countermeasures for) reclined postures, these studies provide guidance on the characteristics of restraint interaction and occupant response that should be targeted for HBM validation. Specifically, these studies highlight the importance of validating a model’s ability to predict spinal kinematics, pelvis kinematics, and lap belt engagement in reclined scenarios, particularly with belt systems designed to mitigate the risk of submarining.

Until recently, no post-mortem human subject (PMHS) reference data was available to evaluate the validity of ATDs and HBMs in reclined postures. In [19] the authors presented a methodology for recline PMHS tests, however no detailed kinetic and kinematic results were presented. This data allowed for initial evaluation of the available HBMs, but no detailed validation was possible [18] [20-21]. Recently, several additional studies were published detailing boundary data, occupant kinematics and injury outcome [22-24]. Additionally, a suite of PMHS corridors for detailed occupant model validation was also made publicly available [25].

The goal of this study is to evaluate the reclined response of state-of-the-art HBMs against data from the previously published reclined PMHS test series conducted at the University of Virginia, USA. Specifically, this study aims to evaluate the response of the Global Human Body Modelling Consortium v.6.0 (GHBMC), Total Human Model for Safety v.6.1 (THUMS), and SAFER Human Body Model v.10 (SAFER) against detailed kinematic data available from published studies. The secondary goal of this study is to identify key differences in HBM and PMHS responses, and to provide recommendations for continued HBM improvement.

II. METHODS

Software and Hardware Used

All simulations in this study were performed using LS-DYNA (R11) Massively Parallel Processing (MPP) explicit FE solver. The simulations were performed on the high-performance computational cluster (Intel Xeon64/sse2). All jobs were run on the same number of nodes.

HBM Sled Environment

The simulation environment, which was described in previous studies [18] [21], matched the setup used in the recently published reclined, full body, PMHS test series [22-24]. It features a semi-rigid simplified seat, a 50° torso recline angle, and a prototype 3-point restraint system. No knee bolster was used. The semi-rigid seat was based on a design developed by [26] and previously used in several PMHS studies [26-27]. The stiffness of the springs was tuned to represent a front seat configuration. The finite element (FE) model of the semi-rigid seat that was developed by Laboratory of Accidentology and Biomechanics/Centre Européen d'Etudes de Sécurité et d'Analyses des Risques (LAB/CEESAR) in cooperation with Partnership for Dummy Technology and Biomechanics (PDB) was further improved by Autoliv Research (Fig. 1), in Sweden. The gravity was applied to all parts of the model through *LOAD_BODY_Z keyword and no global damping was used.

The restraint system used in this study consisted of a 3-point belt equipped with dual lap-belt pretensioners, a shoulder-belt retractor pretensioner, a crash locking tongue, and a shoulder-belt load limiter of 3.5 kN. Anchorage points geometry was designed to represent a seatback-integrated belt configuration. Belt webbing was created using shell seatbelt elements and a 2D slip-ring formulation to facilitate stable and unobstructed belt payout. The FE model of the restraint system, developed by Autoliv Research, comprised of validated component models of production parts. System model was validated by means of sled tests using THOR-50M. The occupant to the environment contact was modelled with the static and dynamic friction coefficient of 0.35 for the seatpan and 0.30 for the belt.

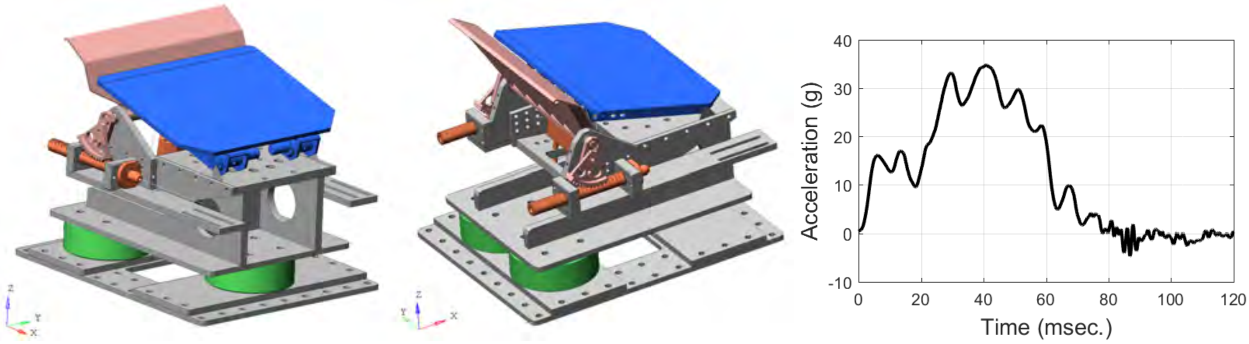

Fig. 1. FE model of semi-rigid seat developed by LAB/CEESAR in cooperation with PDB (left, centre). Full frontal rigid barrier pulse 50 km/h (right) [26]. In the image on the left and the centre, the seatpan is shown in blue, and the anti-submarining pan is shown in light orange. Both of these structures could rotate about a fixed hinge, with the stiffness defined based on a set of springs (tuned to represent the stiffness of a front row automobile seat).

HBM Positioning

Three 50th percentile male HBMs - GHBMC v.6.0, THUMS v.6.1, and SAFER v.10 - were used in this study. All three models represented gross 50th male anthropometry, however they differed in specific local geometry, e.g., pelvic shape and lumbar spine alignment. The GHBMC v.6.0 is the newest iteration of the GHBMC 50th male occupant model, made publicly available in late 2021. It features, among other updates, new softer definition for the adipose tissue and detailed ligamentous lumbar spine model [28]. THUMS v.6.1, released in early 2019, was developed based on previously developed THUMS v.4 model. It features internal organ model and an implementation of active musculature [29]. The SAFER v.10 HBM, originally based on THUMS v.3, features several updates including new models of the head, rib cage, cervical and lumbar spines, pelvis and adipose tissue [30]. The three selected models were validated by means of component tests, table-top experiments and whole body sled tests. All models feature injury prediction capabilities in several body regions [28-30].

Positioning was focused on matching lumbar spine alignment and iliac wing location between HBMs and the PMHS. The HBM positioning was carried out in two separate steps. In the first step the HBMs were positioned roughly by aligning the H-points to the PMHS average, defined based on the centre of the acetabulum (note that with the THUMS v.6.1, a 25mm forward shift in the acetabulum position was needed to account for an apparent smoothing in the local curvature of the acetabulum). The HBMs were then rotated to align their pelvis and lumbar spine angles. This was achieved by matching alignment of a vector passing between the centre of the sacrum and L5 superior endplates (Fig. 2). Next, the HBMs were aligned with the PMHS using average PMHS: L1, L3 and pelvis H-point and iliac crest positions (Fig. 3). These steps were achieved using rigid body transformations of the HBMs.

In the second step the models were positioned with respect to the average PMHS position of L3, L1, T11, T8, T1, head, knee, and calcaneus reported in [22]. Throughout this process the pelvis was constrained to maintain its rigid body alignment from previous steps. Positioning was carried out using the Oasys PRIMER HBM positioning module (Arup, London, England), using a displacement based cable approach. Finally, the HBMs were settled onto the seat by driving a positioned model into the seat to the desired depth of posterior flesh compression (matching top of the iliac crest), with the skeleton constrained so that the bones could not move relative to each other. Gravity settling was initially attempted, but was ultimately not used since it resulted in HBM H-point positions above the average PMHS position (presumably due to the stiffness of the posterior pelvis flesh). Consequently, initial stress and strain in posterior flesh tissue was not considered. The final posture and its comparison with PMHS targets is shown below in Fig. 3 and Table I.

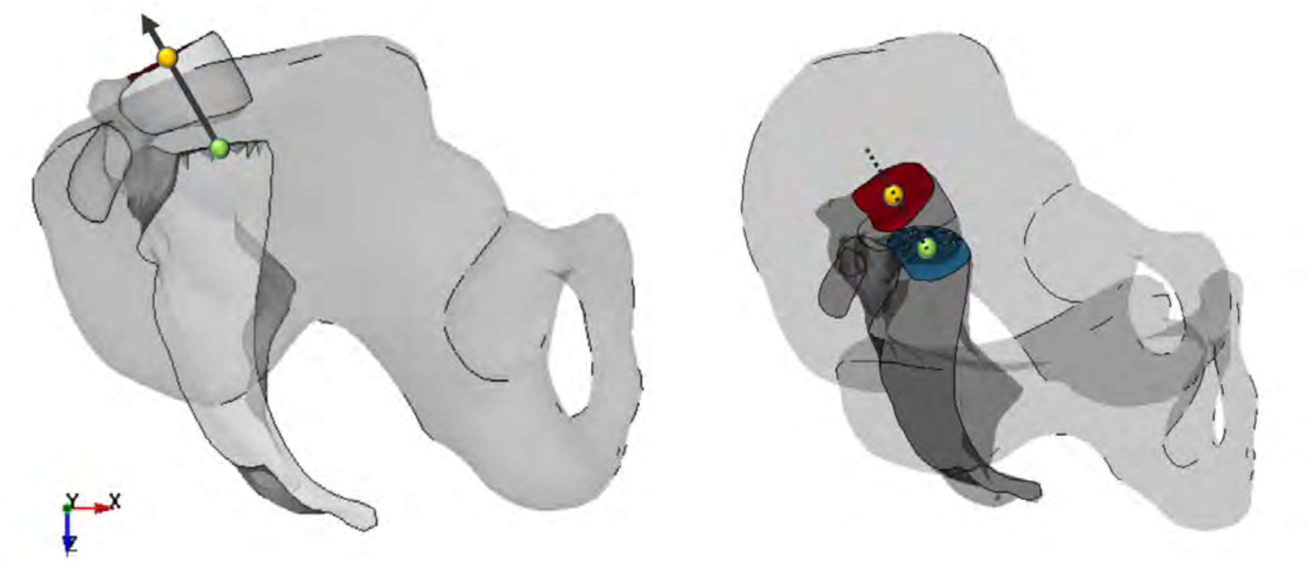

Fig. 2. Definition of a vector passing between the centre of the sacrum and L5 superior endplates used for the HBM alignment across varied anthropometry.

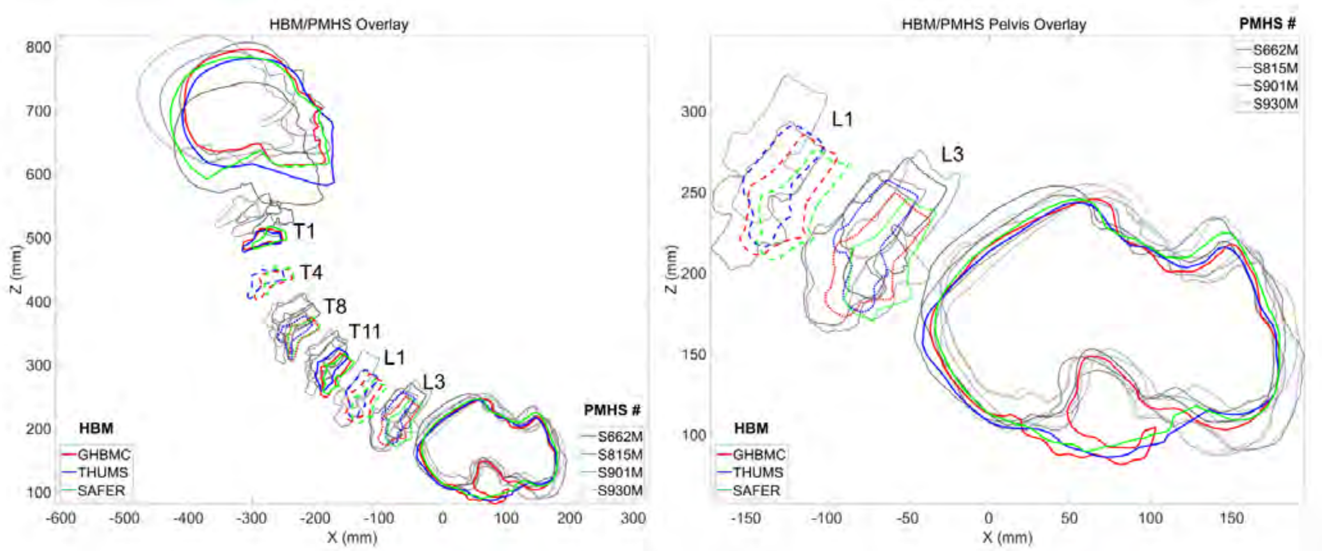

Fig. 3. Comparison of initial HBMs and PMHS spine (left) and pelvis (right). Red silhouette, blue silhouette and green silhouette describe GHBMC, THUMS and SAFER, respectively. The grey silhouettes are the skeletal positions of the individual PMHS tests, reconstructed from bone-mounted motion tracking arrays combined with segmented CT scans. Pelvis, L3, L1, T11, T8, T4, T1 and head outlines included.

Belt Routing

The belts were individually routed across each HBM. For the belt routing the anchorage points were kept constant across all HBMs. The LS-PrePost manual belt routing feature was used for each model. Both the lap and chest belt sections were stretched across each HBM individually to form the shortest belt path using LS-PrePost stretch feature. Even though the same restraint anchorage points were used for all simulations, the lap belt routing differed across the models due to differences in external body shape. The abdominal shapes were the main driving factor behind observed differences. The GHBMC had the most posterior route of the lap belt, followed by THUMS, with SAFER model with the most anterior lap belt location (Fig. 4.).

Table I.

PMHS TARGET POSITIONING AND FINAL HBM POSTURES [22].

Coordinates in FE-Model global coordinate system		Tests (average)				GHBMC		THUMSv6		SAFER	
Position	**Definition**	**X (mm)**	**Z (mm)**	**SD X (mm)**	**SD Z (mm)**	**dx (mm)**	**dz (mm)**	**dx (mm)**	**dz (mm)**	**dx (mm)**	**dz (mm)**
Buck LCS	Seat edge right side	3196.7	461.7	-	-	**0.0**	**0.0**	**0.0**	**0.0**	**0.0**	**0.0**
Head Top	--	3472.0	1264.0	50.1	33.6	**29.2**	**-1.0**	**28.8**	**-14.2**	**33.0**	**-19.0**
Head Origin	Midpoint btw zyg. proc.	3512.5	1137.6	26.7	32.1	**-8.2**	**27.8**	**-31.5**	**-3.1**	**11.8**	**6.5**
T1 Origin	Centre of vertebral body	3467.3	996.3	23.1	15.1	**-9.4**	**-33.6**	**-7.2**	**-36.4**	**-13.0**	**-32.0**
T8 Origin	Centre of vertebral body	3421.4	844.3	8.0	12.2	**-13.0**	**-24.0**	**-4.3**	**-20.7**	**-13.0**	**-24.0**
T11 Origin	Centre of vertebral body	3374.2	787.5	4.4	15.9	**-15.9**	**-24.6**	**-10.7**	**-15.9**	**-19.0**	**-27.0**
L1 Origin	Centre of vertebral body	3320.9	744.1	3.1	22.6	**-9.9**	**-15.9**	**-2.7**	**-9.8**	**-17.0**	**-25.0**
L3 Origin	Centre of vertebral body	3255.0	701.7	14.0	5.9	**1.3**	**-10.1**	**4.9**	**0.7**	**-7.0**	**-12.0**
Pelvis Origin (PSIS)	Midpoint btw L/R PSIS	3191.4	577.0	6.6	12.5	**7.9**	**-1.4**	**-0.3**	**-9.8**	**-2.3**	**-5.8**
Right Knee	Centre lateral epicondyle	2658.7	750.9	19.9	28.2	**17.0**	**26.5**	**-3.5**	**-16.0**	**5.0**	**-8.0**
Left Knee	Centre lateral epicondyle	2660.2	754.1	7.0	28.6						
Right Heel	--	2419.7	350.9	1.9	7.5	**0.2**	**-2.6**	**-12.7**	**-13.0**	**25.0**	**5.0**
Left Heel	--	2418.8	351.2	5.4	12.5						
H-Point	Midpoint btw hip points	3078.0	642.7	1.4	3.3	**10.4**	**-13.4**	**-2.2**	**-7.8**	**-3.4**	**-6.5**

Angle	Definition	Avg. (deg)	SD (deg)	GHBMC Avg. (deg)	THUMSv6 Avg. (deg)	SAFER Avg. (deg)
Pelvis Angle	Pubic symphysis to midpoint btw L/R ASIS wrt the vertical	75.2	5.2	**71.6**	**72.7**	**77.5**
Notch Angle	Mid. btw L/R PSIS to mid. btw L/R ASIS wrt the vertical	45.0	3.5	**39.7**	**53.2**	**51.1**

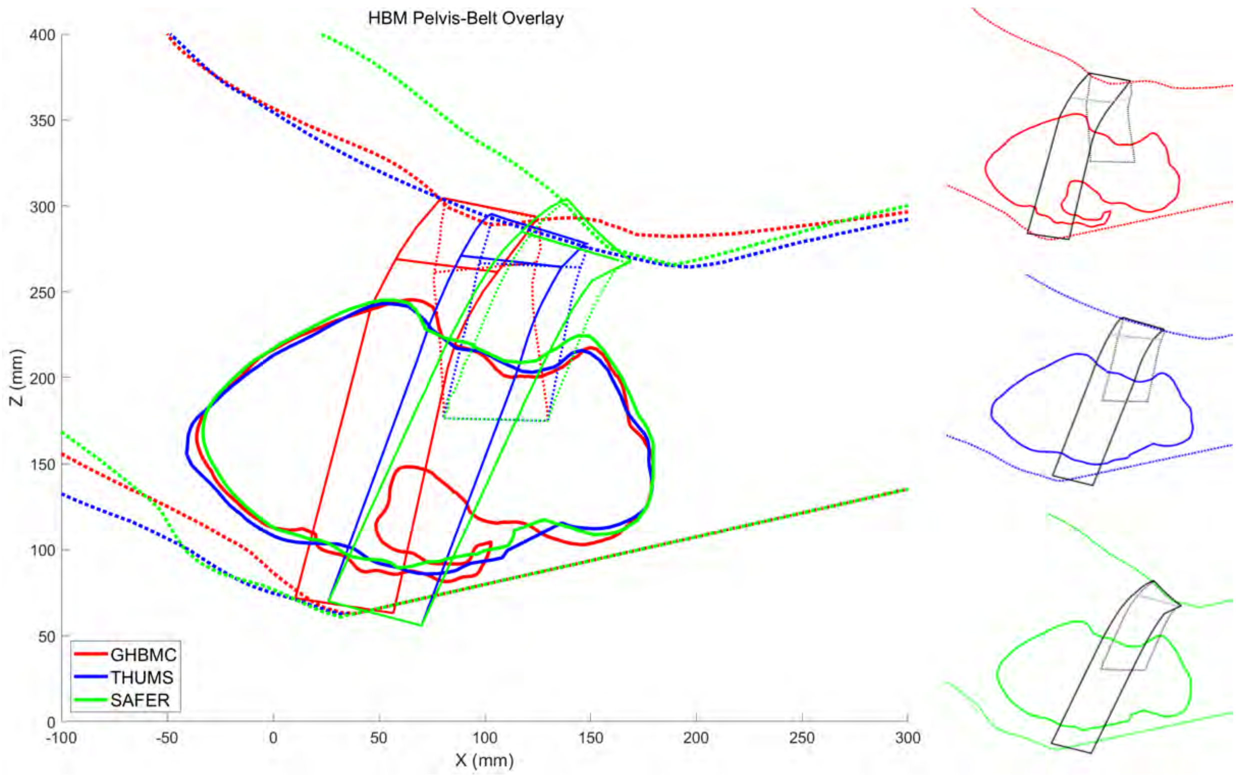

Fig. 4. Initial belt position relative to the occupant's pelvis. The outline of occupant flesh shown.

Data Analysis

Selected HBM results, deemed to be the most relevant for biofidelity evaluation, were compared to previously published PMHS corridors [22]. This included head, T1, T8, T11, L1, L3 and pelvis displacement time histories; head and pelvis rotation time histories, semi-rigid seat/foot pan boundary forces and deflections; and restraint system forces and displacements (Appendix A). The responses were compared qualitatively by overplotting on the corridors, and were compared quantitatively using the CORrelation and Analysis method CORA [31]. For this analysis the total CORA score was calculated with equal weights assigned to corridor score and cross-correlation score. The cross-correlation score was calculated with contributions of 25% from phase and size scores and 50% from progression (shape) score.

III. RESULTS

Simulation Outcome

All HBM simulations were initiated targeting a termination time of 150 ms, and all models reached normal termination.

Kinematics

All three HBMs showed similar kinematics. In all cases no submarining was observed. This is consistent with the referenced PMHS tests, where submarining was not observed in four of the five tests conducted. Consistent with the majority of the PMHS tests, with the HBMs the lap belt effectively constrained the occupant's pelvis, allowing the occupant's torso to lean forward onto the shoulder belt (Fig. 5.).

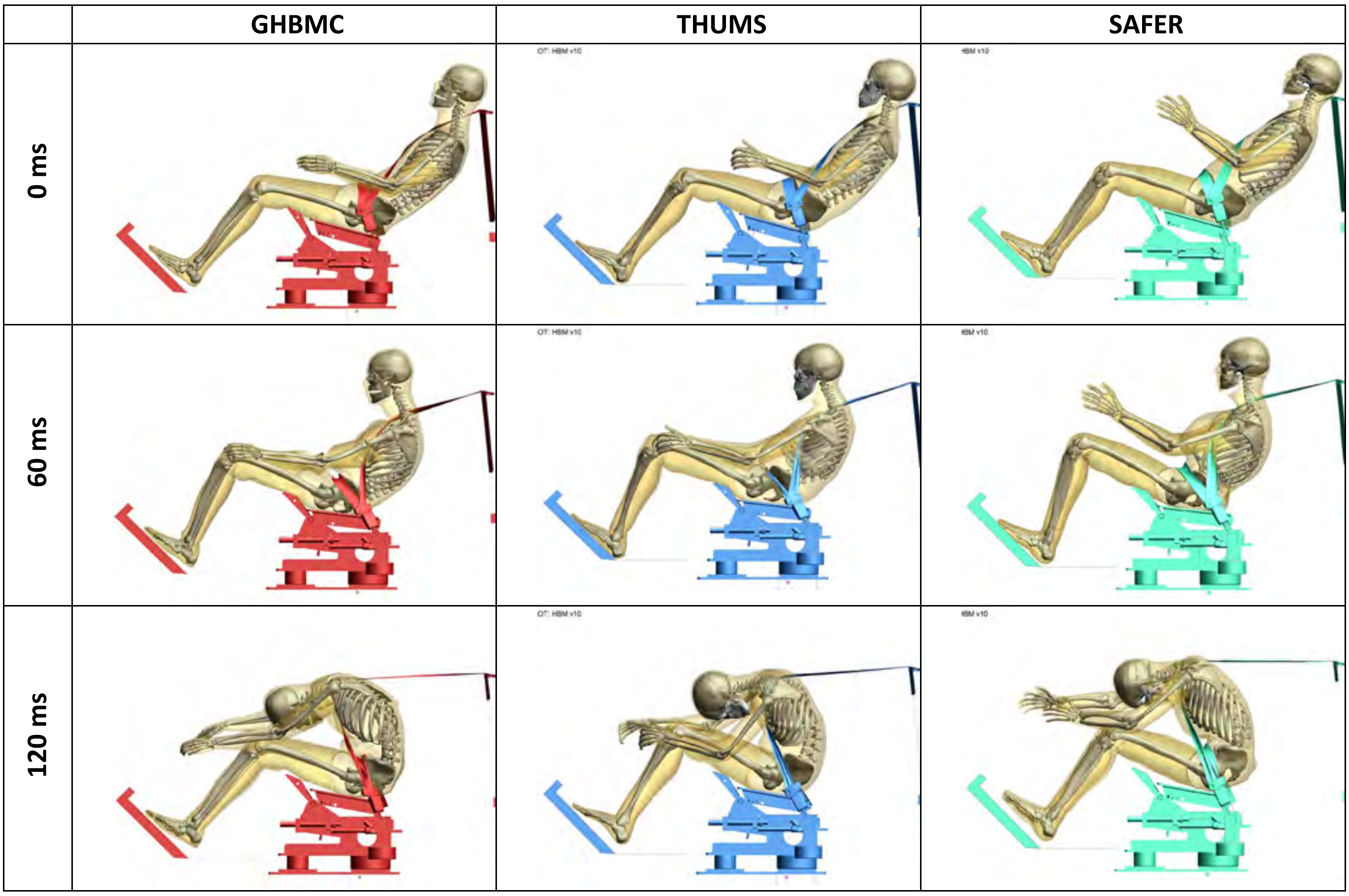

Fig. 5. Still frames extracted from the simulation 0, 60, and 120 ms.

The HBMs' responses were evaluated with respect to previously published PMHS time history corridors (Appendix A) and average PMHS trajectories reconstructed in the XZ plane (Fig. 6 and Fig. 7). All models showed similar pelvis and L3 excursions, comparable with the PMHS average result, however the superior segments (from L1 to head) showed diverging responses. The HBMs' upper body trajectories deviated from the PMHS somewhat, with more downward motion of the head and T1 compared to the PMHS. The upper body segments showed increased forward excursion relative to the average PMHS response for all evaluated HBMs (Fig. 6). It should be noted that the head response corridors (Appendix A) were truncated at 108 ms, since at that time the PMHS head contacted the upper arms, possibly influencing the head's trajectory. The XZ trajectories (Fig. 6 and Fig. 7) were constructed utilising the entire 150 ms of head motion.

The intersegmental alignment analysis (Fig. 7) revealed additional differences between the average PMHS and HBM responses. While both the PMHS and HBMs started with similar spinal alignment (pelvis to head), the subsequent time steps (40, 75, 110 ms, Fig. 7) showed an increased lumbar spine flexion in all HBMs, which was not observed in the PMHS response. The most pronounced difference occurred in the X displacement at the L3, and L1, and T11 levels, resulting in lesser forward displacement when compared to the PMHS average response (Fig. 7) and PMHS corridors (Appendix A).

All HBMs showed a rearward pelvis rotation (away from the lap belt) at peak pelvis forward excursion (75 ms), whereas the PMHS pelvises pitched slightly (approximately 5°.) forward toward the lap belt. All HBMs showed a forward pelvis rotation during a rebound phase (past 90 ms), similar to the PMHS, however this motion was delayed by around 20 ms for GHBMC and THUMS models. The SAFER HBM, was the only model to re-enter the corridor at 90 ms whereas other models remained outside of the pelvis pitch corridor (Appendix A).

Boundary forces and displacements

Boundary forces and displacements (seat, foot pan and belt) generally compared well between the HBMs and the PMHS. Similar magnitude, shape, and phase of forces were measured in the belt, seat, and toepan, though some differences were observed between the models. Small differences (10-20 mm) were also observed in the amount of lap, anchor and shoulder belt pre-tensioning displacement (10-20 ms). Also, the seat pan angular displacement was under-predicted by all HBMs with maximum deflection equal to 9°, comparing to PMHS average result of 11°.

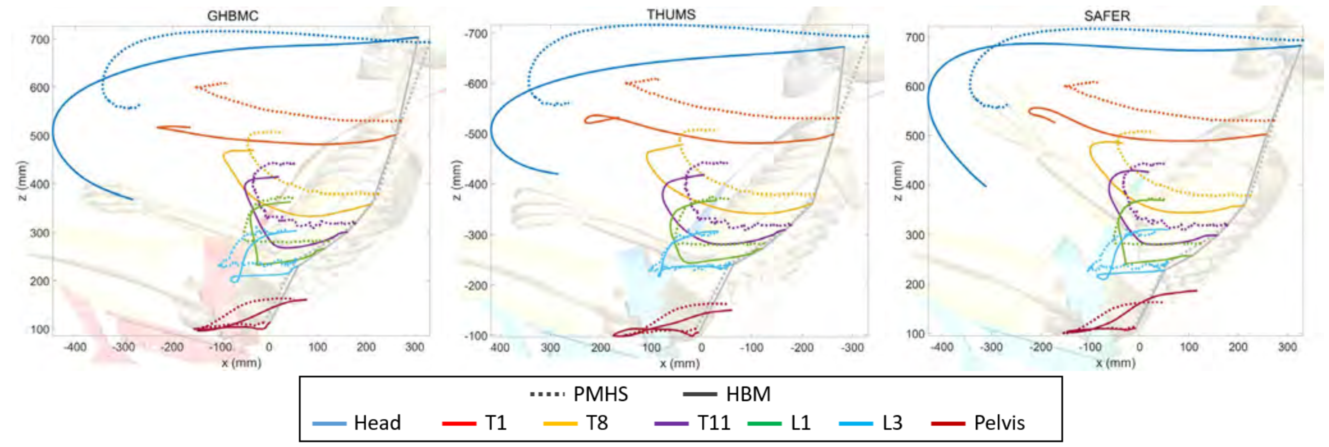

Fig. 6. Head, T1, T8, T11, L3, L1, and pelvis XZ trajectories. HBM vs average PMHS.

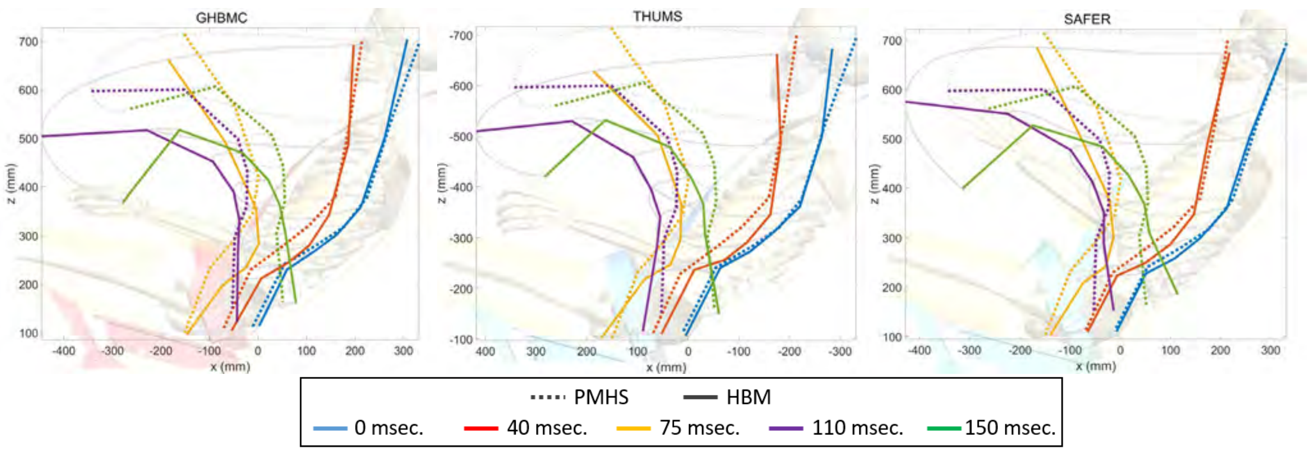

Fig. 7. Intersegmental motions between Head, T1, T8, T11, L3, L1, and pelvis. HBM vs average PMHS.

CORA Analysis

Individual signal CORA scores (Appendix B) were analysed and grouped to provide a better overview of HBMs responses. Average CORA scores were divided into four separate categories. X Avg. and Z Avg. included the average CORA score from head, T1, T8, T11, L1, L3 and pelvis time histories in x and z direction, respectively. Seat average included averaged CORA data from seat pan and anti-submarining pan deflection, seat x and z and foot pan forces. Belt average included CORA scores from shoulder, lap, and anchor belt forces and displacements (Table 2).

X Avg. CORA group showed the highest score out of all the CORA groups considered. This was also true for the total score as well as component, correlation and corridor scores. Z Avg. on the other hand showed the lowest CORA scores across all groups. The only exception was observed for the SAFER model whose Z Avg. corridor score was higher than for the Seat and Belt groups. The Seat and Belt groups were similar across the models and generally ranked between X Avg. and Z Avg. scores. For all CORA groups the corridor scores were the lowest, out of all component scores. For the cross correlation component scores (phase, size and progression) the size score was repeatedly the lowest score (Table II).

Overall, the CORA scores tended to be similar across the three models. Some models tended to fit better for certain individual data traces (for example, the SAFER model tended to fit the Z motion of the head and T1 better), but this was not consistent across all outcome measures or CORA scores. In the end, the aggregate comparison was similar across all three models, with no individual model exhibiting a substantially different performance compared to the PMHS (TABLE III).

Table II.
HBM SPECIFIC AVERAGED CORA SCORES GROUPED INTO FOUR DIFFERENT CATEGORIES.

X Avg.	Corridor Score	Phase Score	Size Score	Progression Score	Correlation Score	Total Score
GHBMC	0.603	0.995	0.854	0.998	0.961	0.782
THUMS	0.452	0.857	0.841	0.996	0.923	0.688
SAFER	0.560	0.984	0.835	0.997	0.953	0.757
Z Avg.	Corridor Score	Phase Score	Size Score	Progression Score	Correlation Score	Total Score
GHBMC	0.332	0.646	0.420	0.877	0.705	0.518
THUMS	0.345	0.714	0.552	0.856	0.744	0.545
SAFER	0.535	0.857	0.561	0.896	0.802	0.668
Seat	Corridor Score	Phase Score	Size Score	Progression Score	Correlation Score	Total Score
GHBMC	0.439	0.846	0.676	0.964	0.862	0.651
THUMS	0.451	0.881	0.783	0.957	0.895	0.673
SAFER	0.448	0.941	0.660	0.967	0.884	0.666
Belt	Corridor Score	Phase Score	Size Score	Progression Score	Correlation Score	Total Score
GHBMC	0.449	1.000	0.760	0.986	0.933	0.691
THUMS	0.308	0.954	0.736	0.982	0.914	0.611
SAFER	0.429	1.000	0.762	0.984	0.932	0.681

TABLE III.
HBM SPECIFIC AVERAGED CORA SORE OF ALL ANALYSED SIGNALS.

	Corridor Score	Phase Score	Size Score	Progression Score	Correlation Score	Total Score
GHBMC	0.475	0.857	0.636	0.943	0.845	0.660
THUMS	0.439	0.871	0.718	0.945	0.870	0.654
SAFER	0.517	0.891	0.682	0.937	0.862	0.689

IV. DISCUSSION

To the best of the authors' knowledge, this is the first study to perform a detailed evaluation of multiple HBMs in the reclined postures matching the available PMHS data. Previous studies, that simulated HBMs in reclined postures, utlised either a preliminary test setup of the reference PMHS tests series [18], or evaluated a single HBM with respect to sub-selected array of PMHS signals [21]. Other studies used conseptualised future vehicle interiors for which no PMHS data are available [9] [13-14]. However, the recently published, detailed PMHS results [22] enables researchers to take a deeper look into validity of these models in recline postures.

Previous studies utlised generalised postures, matching gross geometric features such as torso angle, extremity angles, and H-point location [18]. However, detailed PMHS data offer a wealth of information that may be used to match the HBM postures on the level of specific anthropometric landmarks. In [22], the authors used an optoelectronic stereophotogrammetric system (Vicon) to track individual boney segments throughout the test. This allowed for a projection of computerised tomography (CT) boney reconstructions into modelling space for an in depth view of PMHS postures (Fig. 3). In the course of this study, the authors considered several different HBM pelvis orientations to match the underlying PMHS postures. One idea was to match the Nyquist angle [32], a line connecting the anterior superior iliac spine (ASIS) and the pelvis pubic crest (PC). Another option was to utilise the *notch* angle [33], an angle defined by a line connecting pelvis ASIS and anterior inferior iliac spine (AIIS). Since both of these metrics rely on local measurements, they are very sensitive to local pelvis geometry. An attempt to match these measures lead to large discrepancies in the lumbar spine alignment between the HBMs and when compared with the PMHS. Consequently, alignment of the inferior lumbar spine was chosen as a positioning target, since this approach led to an HBM pelvis alignment that fell within the distribution of initial PMHS pelvis orientations (Fig. 3).

After HBM positioning, initial settling was carried out using gravity, where the models were allowed to settle under their own weight during simulation. This approach resulted in the HBMs' final pelvis position around 20mm above the PMHS target (H-point z-position). This is not surprising, given that these HBMs are not developed nor validated for flesh deformation in low-rate gravity settling. Additionally, the semi-rigid nature of the simplified seat is likely to exacerbate this issue since without seat foam all of the deformation is localised in the HBM flesh. Consequently, the models were forced into desired position.

None of the evaluated HBMs submarined in the current study. This is similar to the PMHS test series result, where submarining was observed in only one out of five tested PMHSs. Additionally, when submarining occurred it was localised only to the inboard side (buckle) of the pelvis [22]. However, in the previous simulation study, the GHBMC v4.5 submarined [18]. Reference [18] speculated that this instance of submarining was associated with the overly stiff HBM flesh, which prevented the lap belt pre-tensioners to effectively position the belt in front of the ASIS. However, the GHBMC v6.0 features a new, softer flesh formulation based on porcine adipose tissue tests data [34]. This new flesh facilitates substantial tissue deformation, allowing pre-tensioners to place the belt in front of the ASIS and effectively preventing submarining.

Although the method used to route the lap belt was consistent across the HBMs, differences in the external surface contour of the HBMs resulted in a somewhat different geometry of the lap belt (Fig. 4). This was due to the fact that each model had a different abdominal flesh distribution, forcing the belt closer to or further away from the ASIS. While this has a potential to skew the submarining outcome, none of the HBMs submarined in this study. However, in the future studies, the HBM abdominal flesh can be morphed to change the initial belt placement and investigate its effect on submarining sensitivity.

All models showed relatively good agreement with PMHS X direction time histories (horizontal), however the discrepancies in Z directions (vertical) were larger. This occurred for body segments above L1 (Fig. 6 and Table 2). As a specific example, XZ time histories for head (Fig. 8) and T1 (Fig. 9) were extracted from the Appendix A and presented below. Although the X direction trajectory corridor was quite narrow compared to the other corridors, the HBMs showed relatively good agreement with the PMHS until about 80 ms (after which the HBMs tended to over-predicted the forward excursion; Fig. 8 and Fig. 9). Interestingly, THUMS head X direction trajectory showed the best agreement with the PMHS corridor. However, for the Z direction trajectory, all HBMs showed a diverging response throughout the entire time history. While the PMHS responses showed initial neutral or upward (negative Z) motion for segments from L1 to head, all HBMs showed initial downward motion (positive Z) (Fig. 8, Fig. 9 and Appendix A).

These observations are likely a consequence of an increased flexion of the lumbar spine shown by all HBMs, compared to lumbar flexion observed in the PMHS (as observed through motion tracking with bone-mounted marker arrays; [22]). This is especially visible in Fig. 7. at 75 ms. While the average PMHS lumbar spine (section from L3 to T11) remained straight, all HBMs showed substantial lumbar spine flexion. This discrepancy is likely responsible for differences in upper body kinematics. An increased flexion at the lumbar spine leads to a longer (curved) path of the adjacent spinal segments. This resulted in more downward motion of the upper body segments than the PMHS. Interestingly, a recent study appeared to show similar results with the GHBMC [35], where the model exhibited an increased lumbar spine flexion, however HBM data for detailed comparison of the lumbar spine motion with the PMHS was not provided.

Increased lumbar spine flexion is also likely responsible for the discrepancies observed in the pelvis rotation. While all models predicted the pelvis forward excursion, the pelvis pitch (anterior-posterior rotation) showed systematic difference between the PMHS and HBMs (Fig. 10.). The PMHS showed minimal or no posterior rotation (positive signal - ASIS rotating away from the belt) of the pelvis. However, the HBMs rotated posteriorly at the peak pelvis forward excursion (70-80 ms). This effect is also visible in the pelvis-L3 segment alignment in Fig. 7. (75 ms).

This data suggests that the differences between the PMHS and HBMs is a consequence of the lumbar spine response. This is not surprising given the fact that there is limited PMHS data that can be used for development and validation of this body region. Previous studies used for HBM development were characterised either by complex boundary conditions and lack of kinematic outputs [36] or by a limited range of forces, moments and displacements [37]. While previous studies might have been sufficient for a HBM development applicable to upright postures, where such discrepancies were not observed, they might lack the range of applicability for scenarios with high lumbar flexion, such as recline. This could result in a lumbar spine model that is too compliant under large flexion load. It is also possible, that for the PMHS, there exists an alternative load path offloading the lumbar spine that is not yet captured by the HBM. The question of load sharing between lumbar spine and abdominal flesh and viscera, especially in cases with large flexion moments, is not yet well understood. This load sharing within the trunk is likely to have a profound effect on the flexion in the spine, the motion of the pelvis, and the motion of the upper body, and may be affected by complex mechanical phenomena such as the semi-compressible internal pressure dynamics of the abdominal and thoracic viscera. Given the importance and potential complexity of this interaction, this internal load sharing within the trunk represents a substantial research question that should be addressed in future HBM validation and refinement efforts. Another possible source of observed discrepancies could be associated with the pelvic flesh definition within the models. A stiffer posterior flesh, as identified during settling simulations, may influence the pelvis interacting with a seatpan. A stiffer flesh may be less susceptible to compression during lap belt pretensioning, resulting in reduced coupling of the pelvic bone with the seatpan, and allowing for posterior pelvis rotation.

The authors would like to point out that the results of CORA analysis should be used only to compare HBMs relative to each other. These CORA scores should not be used to draw definitive conclusions about the applicability of these models to the frontal reclined scenario. The final CORA score may be influenced by many factors such as selection of data traces to analyse, the selection of the time period over which they are analysed, the specific construction of the construction of corridors, and the selection of component score weights. For example, it is possible that a valid and useful model could end up with a low partial CORA score due to specific anthropometric difference, that was not covered by the tested PMHS. This is why these scores should not be accepted blindly in the evaluation of model applicability, but rather should be used as a tool to compare the relative fit of different models, and to identify potential differences that may be targeted for further investigation.

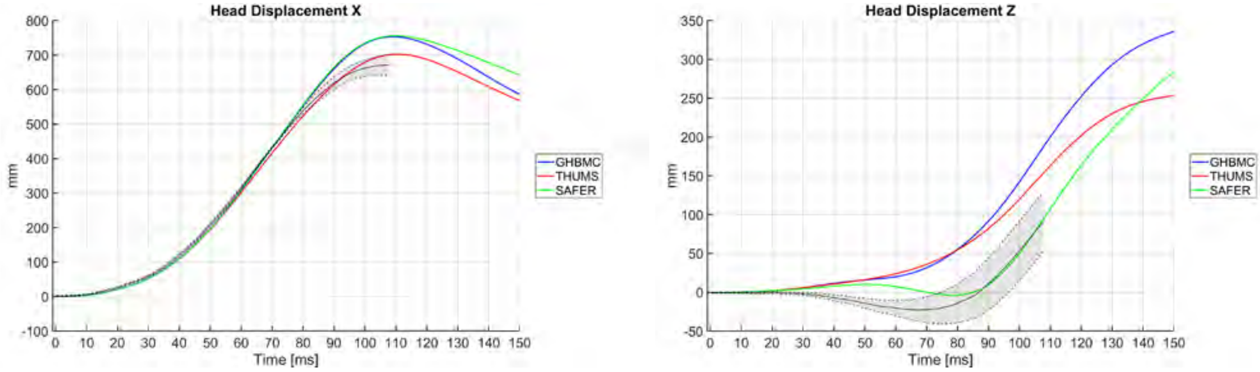

Fig. 8. Head X and Z time histories. PMHS corridor vs HBM results.

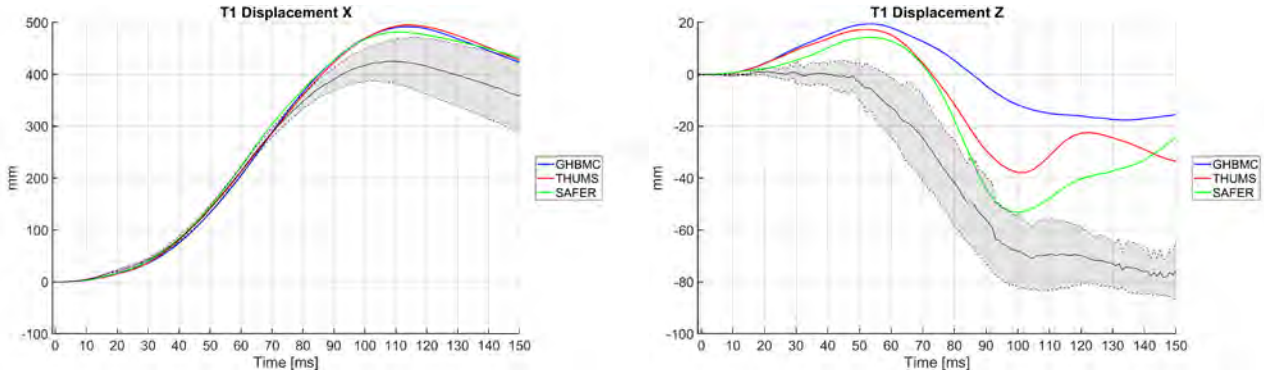

Fig. 9. T1 X and Z time histories. PMHS corridor vs HBM results.

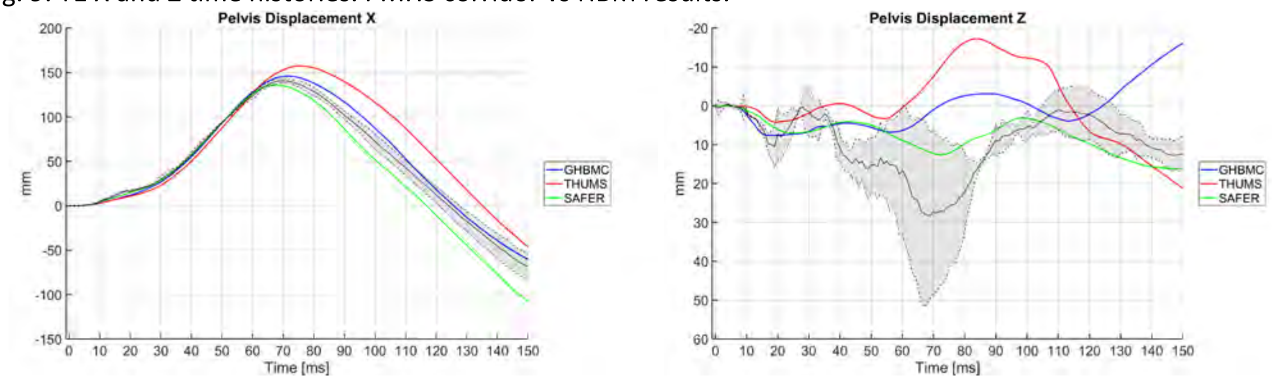

Fig. 10. Pelvis X displacement and Y rotation time histories. PMHS corridor vs HBM results.

Finally, many of the factors investigated here are also likely to have effects across a diverse range of occupants. Submarining risk is likely to be affected by body shape and soft tissue distribution, both of which are different between males and females. Fundamental differences in skeletal shape (especially in the pelvis) may also influence restraint interaction and skeletal motion. Restraint interaction is also likely affected by factors such as Body Mass Index or obesity, which can further influence the overall body shape and the engagement between the restraints and skeleton [38-39]. Finally, skeletal kinematics and injury risk may be influenced by factors affecting the relative stiffness between the body segments, ranging from hormonal effects on the laxity of connective tissues to bridging spinal ossifications and bone mineral density loss associated with advanced age. Considering the potential sensitivity to body shape and skeletal geometry, future work should include extending this investigation to collection of biofidelity reference data for other population segments, e.g., mid-sized females, and development and evaluation of HBMs using such data.

V. Conclusions

This is a first study to provide an in depth, signal-by-signal, evaluation of multiple HBMs in a reclined posture in frontal crashes, compared against reclined PMHS tests. This evaluation is critical for understanding of the validity and limitations of the HBMs in designing novel restraint systems for reclined occupants. The following conclusions can be drawn from this study:

- All HBMs showed similar performance relative to the PMHS test data, with total CORA scores of 0.660 for the GHBMC v.6.0, 0.654 for the THUMS v.6.1, and 0.689 for the SAFER HBM v.10.

- All HBMs showed good lap belt engagement and no submarining was observed.
- All models showed similar X-axis motion of the head, T1, and pelvis compared to the PMHS.
- All models showed larger differences with Z direction trajectories, where the models showed more downward motion of the head and T1 compared to the PMHS. The SAFER model showed the smallest difference and this was reflected in both Z Avg. and Total CORA score.
- All models showed a posterior rotation of the pelvis at the maximum forward excursion. This was not observed in the PMHS data
- All models showed localised lumbar spine flexion throughout the tests. This was not observed in PMHS data where the lumbar spine remained in relatively consistent alignment throughout the test. This was likely a contributing factor to posterior pelvis rotation and under-prediction of Z direction trajectories in the HBMs.
- Considering the differences observed in both the model settling and dynamic response, the results suggest that further refinement may be warranted in the stiffness of the posterior pelvis flesh (affecting the model settling) and lumbar flexion stiffness (affecting the pelvis motion and upper body kinematics). Further investigation may be warranted in the relative load sharing between the lumbar spine and the abdominal soft tissue, beginning with experimental study to develop targets for human body models.

VI. References

[1] SAE On-Road Automated Vehicle Standards Committee, (2014) Taxonomy and definitions for terms related to on-road motor vehicle automated driving systems. SAE International.

[2] U.S. Department of Transportation, 2017. Automated Driving Systems 2.0 - A Vision for Safety. Available at: https://www.nhtsa.gov/sites/nhtsa.dot.gov/files/documents/13069a-ads2.0_090617_v9a_tag.pdf [Accessed February 21, 2019].

[3] U.S. Department of Transportation, 2017. Automated Driving Systems 3.0 - Preparing for the Future of Transporttation. Available at: https://www.transportation.gov/sites/dot.gov/files/docs/policy-initiatives/automated-vehicles/320711/preparing-future-transportation-automated-vehicle-30.pdf [Accessed February 21, 2019].

[4] Martin Östling, M., Larsson, A. (2019) Occupant activities and sitting positions in automated vehicles in china and sweden, 26th Enhanced Safety of Vehicles, Netherlands, Paper Number 19-0083.

[5] Jorlöv S., Bohman K., and Larsson A. (2017) Seating Positions and Activities in Highly Automated Cars–A Qualitative Study of Future Automated Driving Scenarios. In Proceedings of IRCOBI conference. Antwerp, Belgium.

[6] Liers, H. and Unger, T., 2019. Prediction of the expected accident scenario of future Level 2 and Level 3 cars on German motorways. *Proceedings of International Research Council on Biomechanics of Injury (IRCOBI)*.

[7] Saadé, J., Chajmowicz, H. and Cuny, S., 2019. Prospective Evaluation of the Effectiveness of Autonomous Emergency Braking Systems in Increasing Pedestrian Road Safety in France. In *Proceedings of IRCOBI Conference*.

[8] National Transportation Safety Board, 2017. Collision between a Car Operating with Automated Vehicle Control Systems and a Tractor-Semitrailor Truck near Williston, Florida, 7 May 2016.

[9] Forman, J., Lin, H., Gepner, B., Wu, T., Panzer, M. (2018) Occupant safety in automated vehicles: effect of seatback recline on occupant restraint. Japan Society of Automotive Engineers.

[10] Lin, H., Gepner, B., Wu, T., Forman, J. and Panzer, M., 2018. Effect of seatback recline on occupant model response in frontal crashes. In Proceedings IRCOBI Conference.

[11] Matsushita, T., Saito, H., Sunnevång, C., Östling, M., Vishwanatha, A. and Tabhane, A., 2019. Evaluation of the protective performance of a novel restraint system for highly automated vehicles (HAV).

[12] Gepner, B., Rawska, K., et al., 2019 Challenges for Occupant Safety in Highly Automated Vehicles Across

Various Anthropometries. In 26th International Technical Conference on the Enhanced Safety of Vehicles (ESV), In press. 2019. Eindhoven, Netherlands

[13]Rawska, K., Gepner, B., et al., 2019, Submarining Sensitivity across Varied Anthropometry in Autonomous Driving System Environment. Traffic injury prevention,

[14]Rawska, K., Gepner, B., Moreau, D. and Kerrigan, J.R., 2020. Submarining sensitivity across varied seat configurations in autonomous driving system environment. *Traffic injury prevention*, *21*(sup1), pp.S1-S6.

[15]Kerrigan, J., Rawska, K., et al., 2019, Preventing Submarining for Reclined Occupants of Autonomous Vehicles. Japan Society of Automotive Engineers

[16]Boyle, K. J., Reed, M. P., Zaseck, L. W., & Hu, J. (2019). A human modelling study on occupant kinematics in highly reclined seats during frontal crashes. In Proceedings of the International Research Conference on the Biomechanics of Impact, IRCOBI, Florence, Italy, 11th September-13th September. IRC-19-43.

[17]Ji, P., Huang, Y., & Zhou, Q. (2017). Mechanisms of using knee bolster to control kinematical motion of occupant in reclined posture for lowering injury risk. International journal of crashworthiness, 22(4), 415-424.

[18]Gepner, B.D., Draper, D., Mroz, K., Richardson, R., Ostling, M., Pipkorn, B., Forman, J.L. and Kerrigan, J.R., 2019, Comparison of Human Body Models in Frontal Crashes with Reclined Seatback. In Proceedings of International Research Council on the Biomechanics of Injury.

[19]Richardson, R., Donlon, JP., et al., 2019, Test Methodology for Evaluating The Reclined Seating Environment With Human Surrogates. In 26th International Technical Conference on the Enhanced Safety of Vehicles (ESV), In press. 2019. Eindhoven, Netherlands

[20]Gepner, B.D., Toczyski, J., Rawska, K., Moreau, D. and Kerrigan, J.R., Sensitivity of Human Body Model Response Relative to the Lumbar Spine and Pelvic Tissue Formulation.

[21]Mroz, K., Östling, M., Richardson, R., Kerrigan, J., Forman, J., Gepner, B., Lubbe, N. and Pipkorn, B., 2020. Effect of Seat and Seat Belt characteristics on the Lumbar Spine and Pelvis Loading of the SAFER Human Body Model in reclined Postures. In *Proceedings of the IRCOBI Conference*.

[22]Richardson, R., Donlon, J.P., Jayathirtha, M., Forman, J.L., Shaw, G., Östling, M., Mroz, K. and Pipkorn, B., 2020. Kinematic and injury response of reclined PMHS in frontal impacts. *Stapp car crash journal*, *64*, pp.83-153.

[23]Richardson, R., Jayathirtha, M., Chastain, K., Donlon, J.P., Forman, J., Gepner, B., Östling, M., Mroz, K., Shaw, G., Pipkorn, B. and Kerrigan, J., 2020. Thoracolumbar spine kinematics and injuries in frontal impacts with reclined occupants. *Traffic injury prevention*, *21*(sup1), pp.S66-S71.

[24]Richardson, R., Jayathirtha, M., Donlon, J.P., Forman, J., Gepner, B., Ostling, M., Mroz, K., Pipkorn, B. and Kerrigan, J.R., 2020. Pelvis Kinematics and Injuries of Reclined Occupants in Frontal Impacts. In *Proceedings of the International Research Conference on the Biomechanics of Impact, IRCOBI. IRC-20-60*.

[25]University of Virginia, Center for Applied Biomechanics (2021) Positioning Data for Human Body Models in Reclined Seating. Available at: https://virginia.app.box.com/s/u58cl0s9zfpsgbo54h28xobq1i47nxln [Accessed: 20 April 2021].

[26]Uriot, J., Potier, P., Baudrit, P., Trosseille, X., Petit, P., Richard, O., Compigne, S., Masuda, M. and Douard, R., 2015. Reference PMHS Sled Tests to Assess Submarining (No. 2015-22-0008). SAE Technical Paper.

[27]Trosseille, X., Petit, P., Uriot, J., Potier, P., Baudrit, P., Richard, O., Compigne, S., Masuda, M. and Douard, R., 2018. Reference PMHS sled tests to assess submarining of the small female. Stapp car crash journal, 62, pp.93-118.

[28]GHBMC, Global Human Body Models Consortium User Manual: Simplified Pedestrians Versions 1.5.3, 1.6.3, 2.4.3 for LS-DYNA®, Elemance LLC, October 2020.

[29]Kato, D., Nakahira, Y., Atsumi, N. and Iwamoto, M., 2018, September. Development of human-body model

THUMS Version 6 containing muscle controllers and application to injury analysis in frontal collision after brake deceleration. *In IRCOBI Conference* (pp. 207-223).

[30]Östh, J., Pipkorn, B., Forsberg, J. and Iraeus, J., 2021. Numerical reproducibility of Human Body Model crash simulations. *In Paper submitted to IRCOBI Conference*.

[31]Gehre, C., Gades, H. and Wernicke, P., 2009, June. Objective rating of signals using test and simulation responses. In *21st International Technical Conference on the Enhanced Safety of Vehicles Conference (ESV)* (pp. 09-0407).

[32]Nyquist, G.W. and Patrick, L.M., 1976. Lumbar and pelvic orientations of the vehicle seated volunteer. *SAE Transactions*, pp.2610-2621.

[33]Moreau, D., Donlon, J.P., Chebbi, A., Jayathirtha, M., Sochor, S., Overby, B., Richardson, R., Gepner, B., Forman, J., Östling, M. and Kerrigan, J., A Methodology to Replicate Lap Belt Loading Conditions from a Sled Impact Test in a Non-Impact Dynamic Environment on Whole-Body Postmortem Human Subjects.

[34]Comley, K. and Fleck, N., 2012. The compressive response of porcine adipose tissue from low to high strain rate. *International Journal of Impact Engineering*, *46*, pp.1-10.

[35]Grébonval, C., Trosseille, X., Petit, P., Wang, X. and Beillas, P., 2021. Effects of seat pan and pelvis angles on the occupant response in a reclined position during a frontal crash. *PloS one*, 16(9), p.e0257292.

[36]Demetropoulos, C.K., Yang, K.H., Grimm, M.J., Artham, K.K. and King, A.I., 1999. High rate mechanical properties of the Hybrid III and cadaveric lumbar spines in flexion and extension (No. 99SC18). *SAE Technical Paper*.

[37]Heuer, F., Schmidt, H., Klezl, Z., Claes, L. and Wilke, H.J., 2007. Stepwise reduction of functional spinal structures increase range of motion and change lordosis angle. *Journal of biomechanics*, *40*(2), pp.271-280.

[38]Forman, J., Lopez-Valdes, F. J., Lessley, D., Kindig, M., Kent, R., & Bostrom, O. (2009, October). The effect of obesity on the restraint of automobile occupants. In Annals of Advances in Automotive Medicine/Annual Scientific Conference (Vol. 53, p. 25). Association for the Advancement of Automotive Medicine.

[39]Reed, M. P., Ebert-Hamilton, S. M., & Rupp, J. D. (2012). Effects of obesity on seat belt fit. Traffic injury prevention, 13(4), 364-372.

VII. APPENDIX

APPENDIX A

Comparison of HBM response with the selected PMHS corridors.

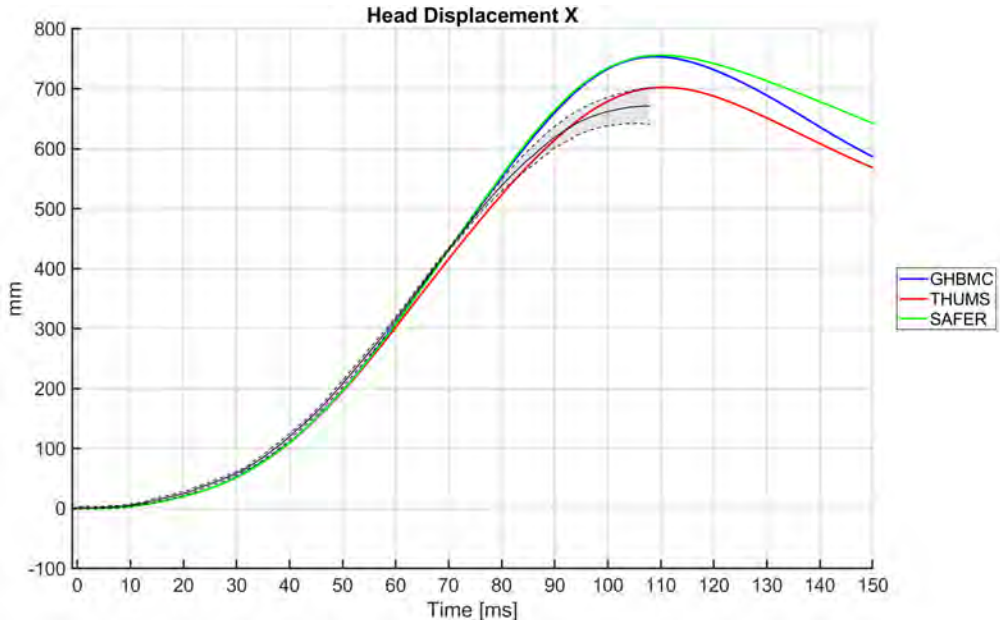

Figure A 1: Head displacement X

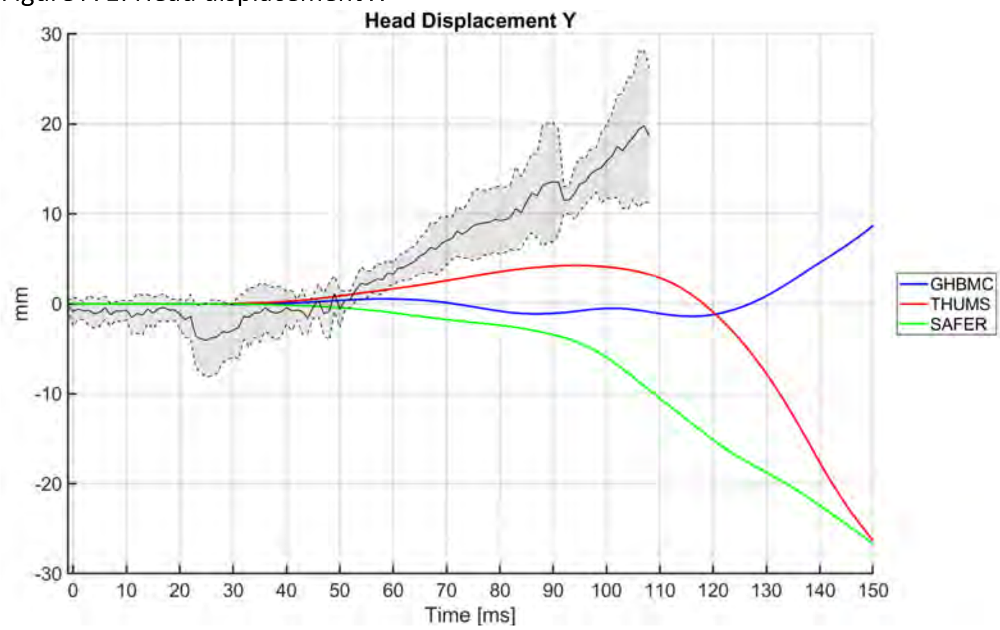

Figure A 2: Head displacement Y

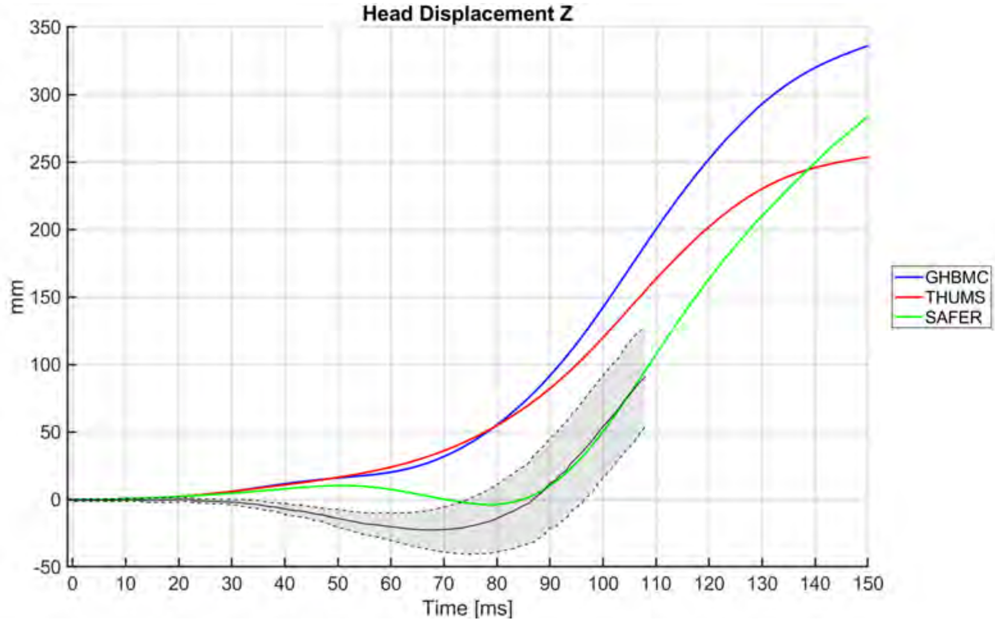

Figure A 3: Head displacement Z

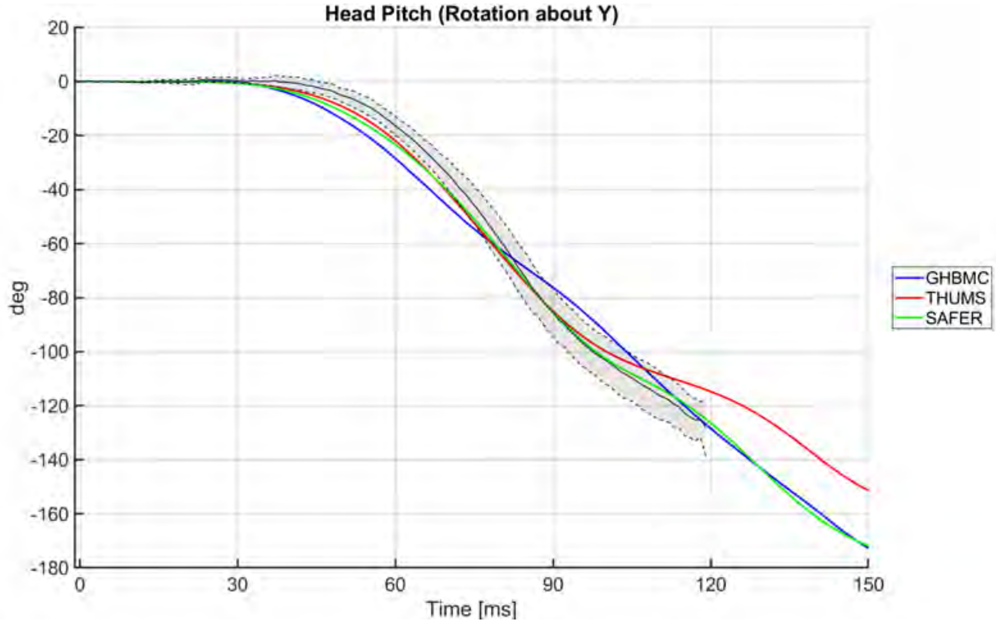

Figure A 4: Head pitch

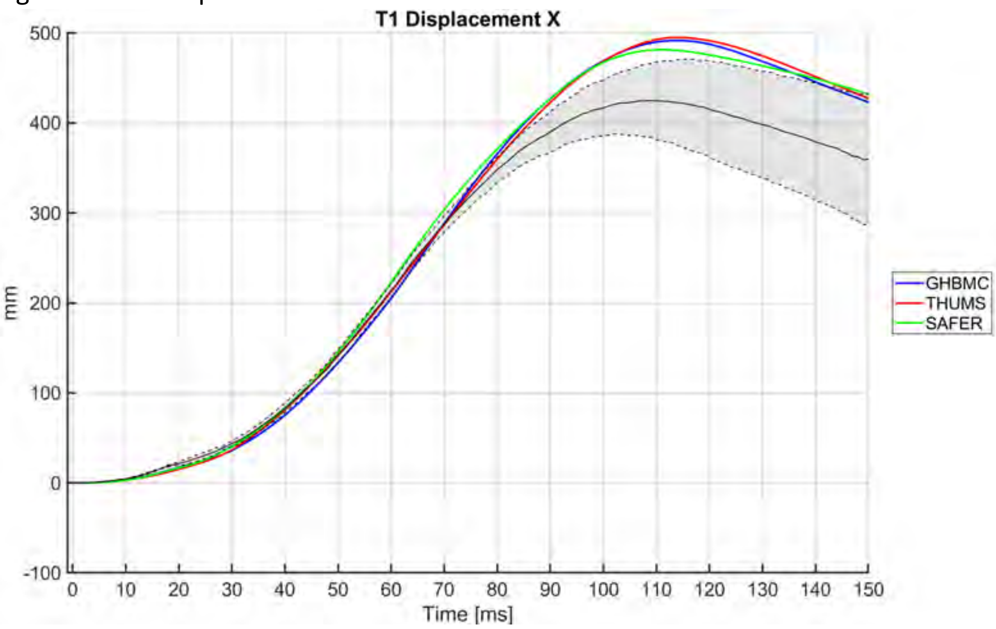

Figure A 5: T1 displacement X

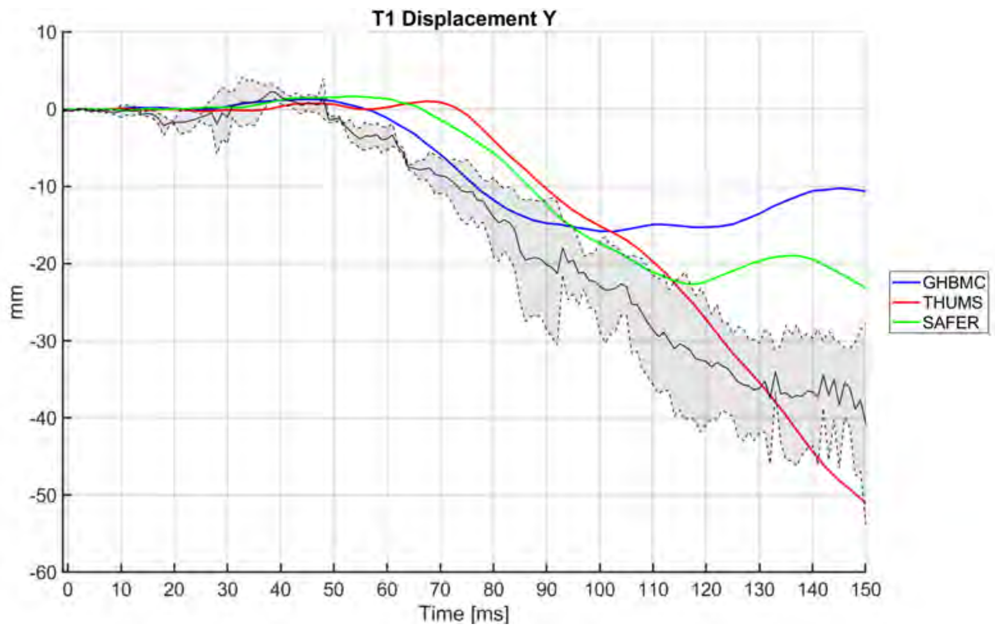

Figure A 6: T1 displacement Y

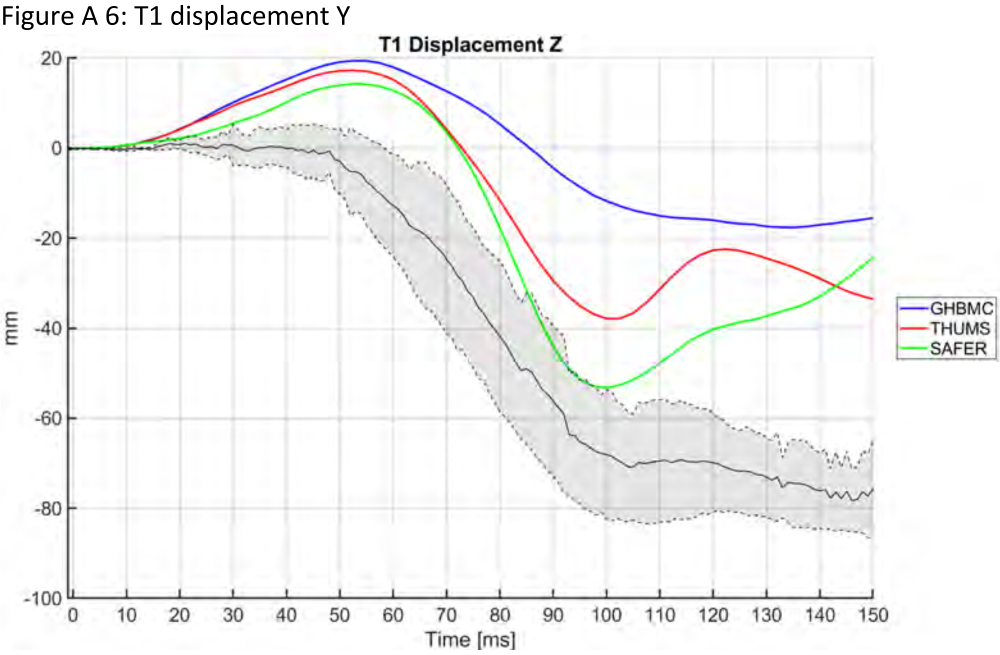

Figure A 7: T1 displacement Z

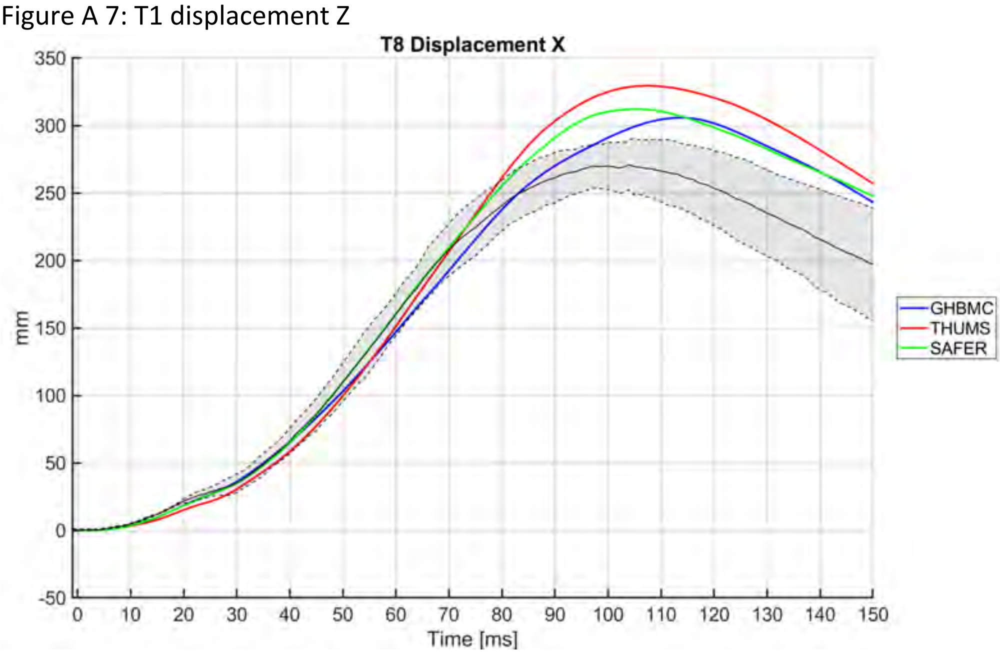

Figure A 8: T8 displacement X

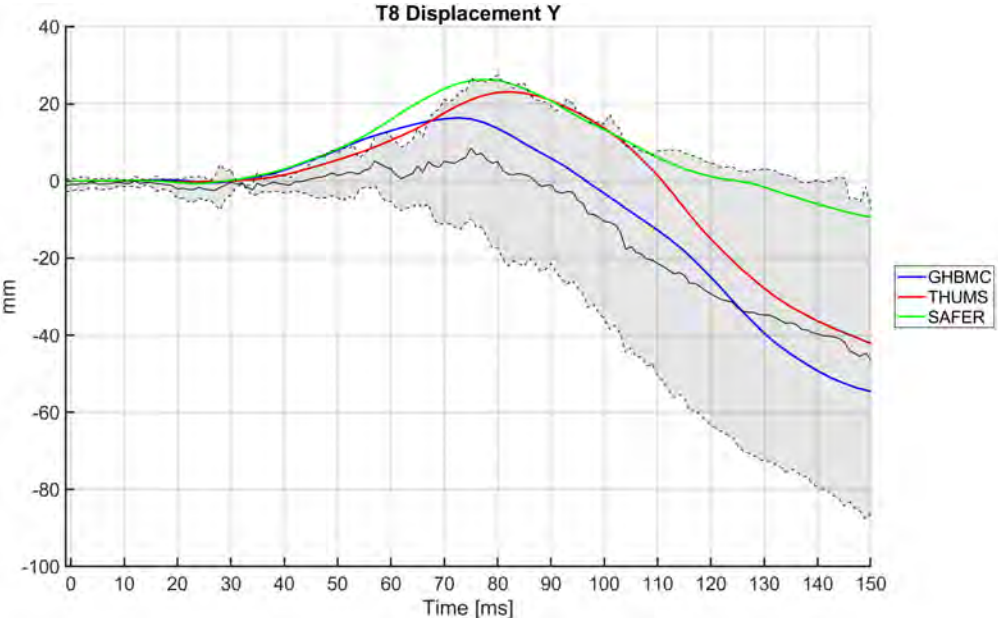

Figure A 9: T8 displacement Y

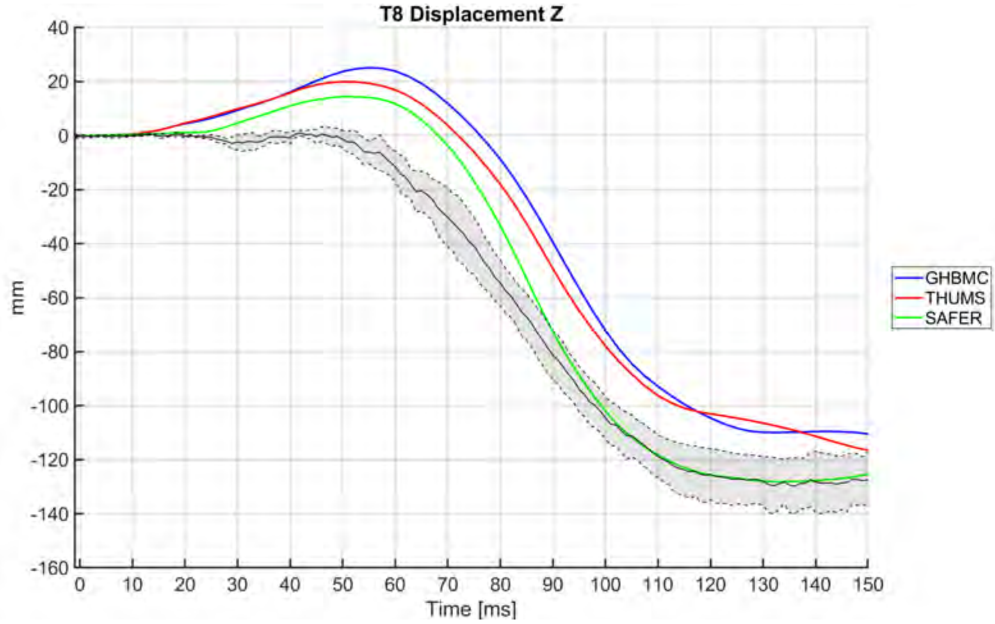

Figure A 10: T8 displacement Z

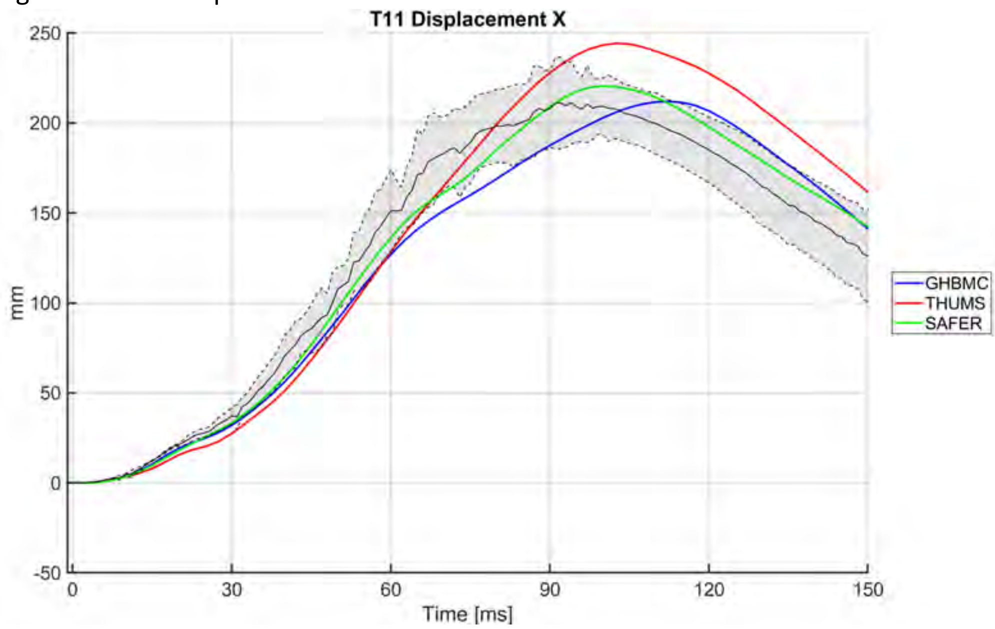

Figure A 11: T11 displacement X

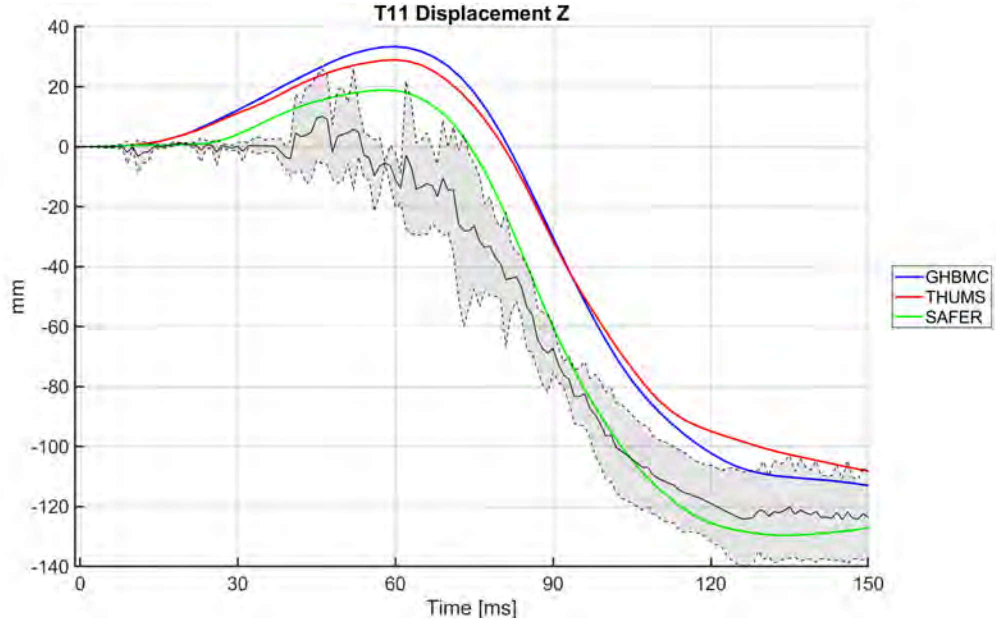

Figure A 12: T11 displacement Y

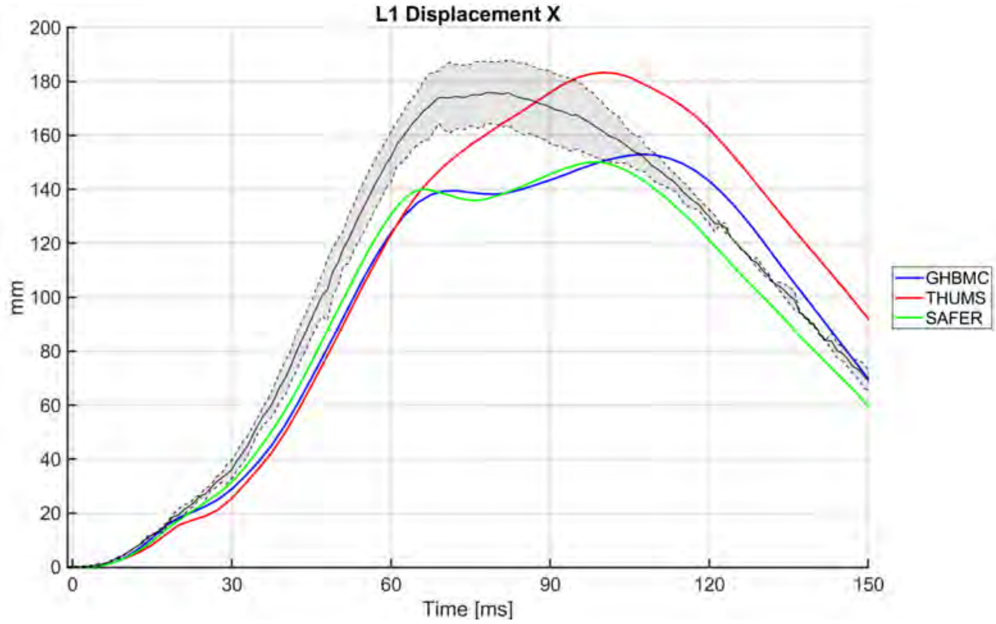

Figure A 13: L1 displacement X

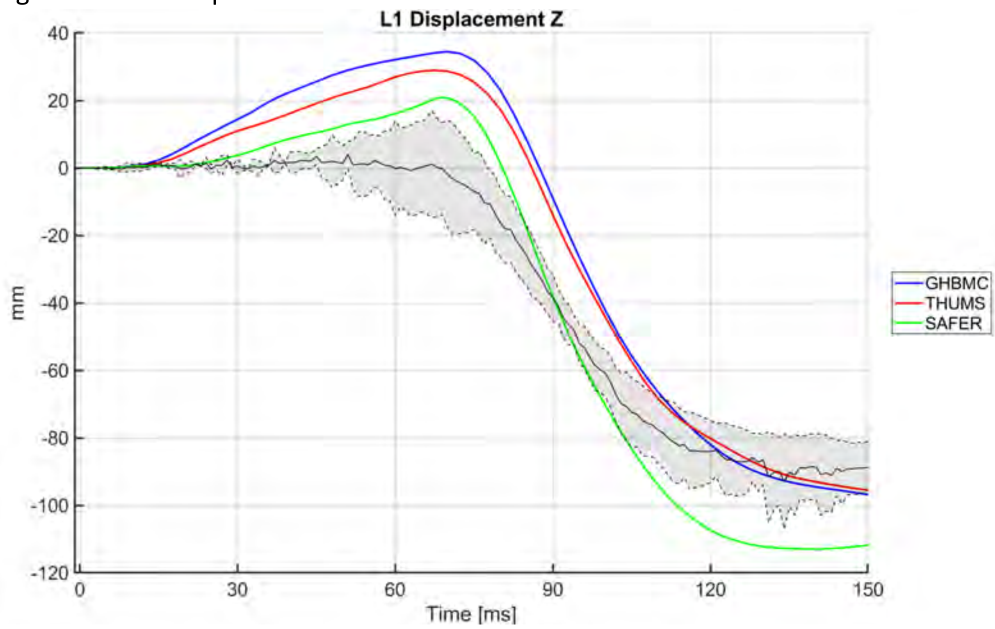

Figure A 14: L1 displacement Z

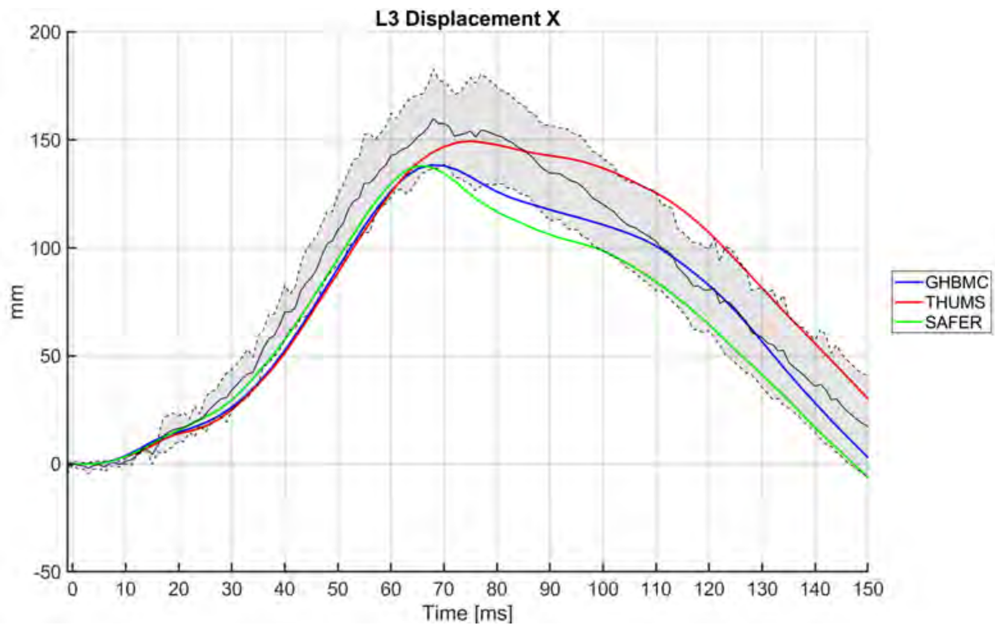

Figure A 15: L3 displacement X

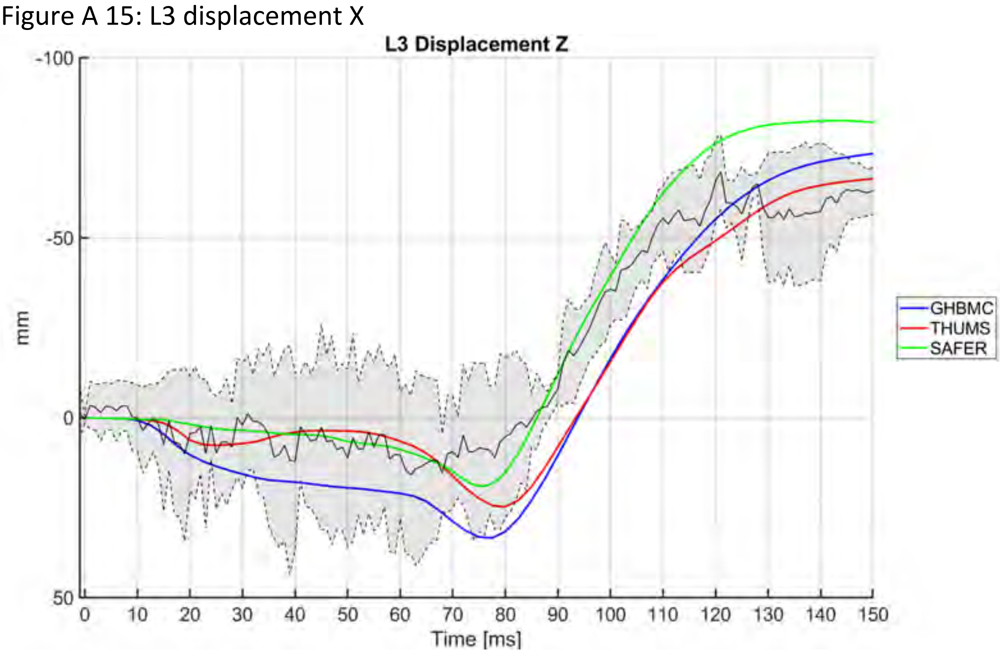

Figure A 16: L3 displacement Z

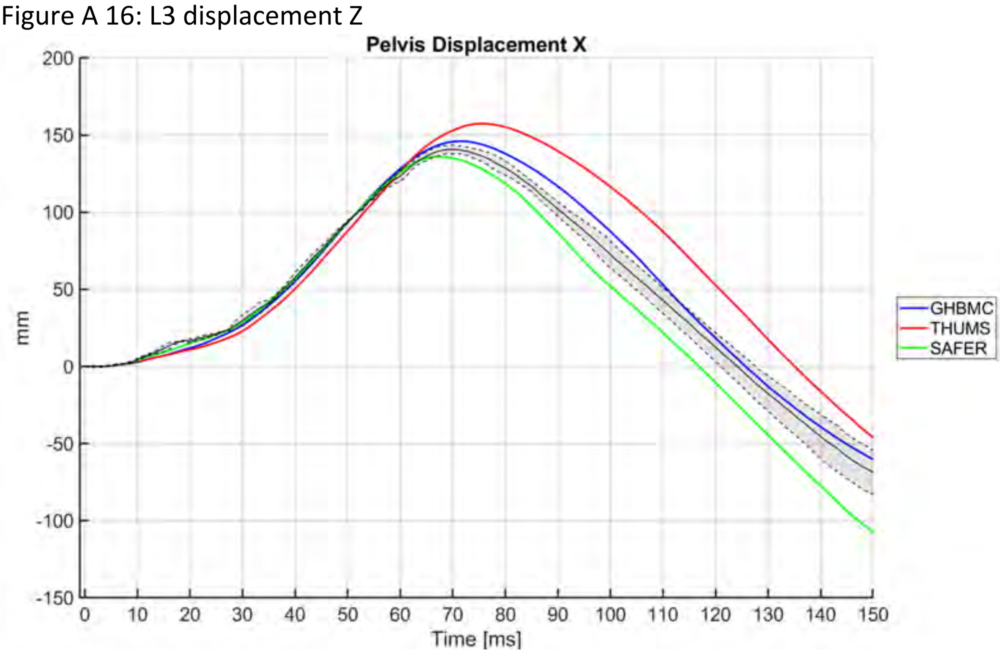

Figure A 17: Pelvis displacement X

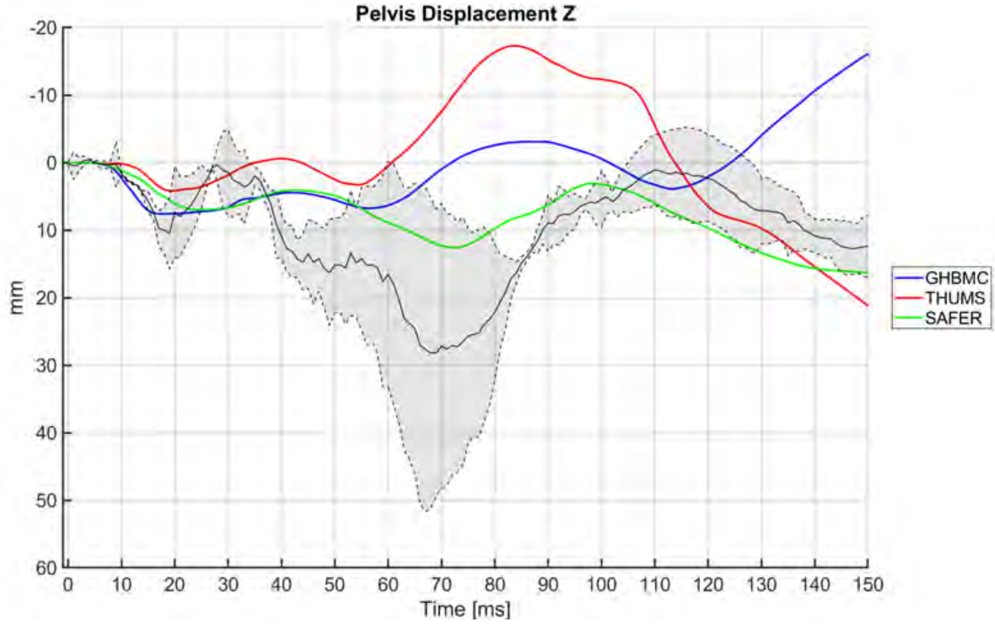

Figure A 18: Pelvis displacement Z

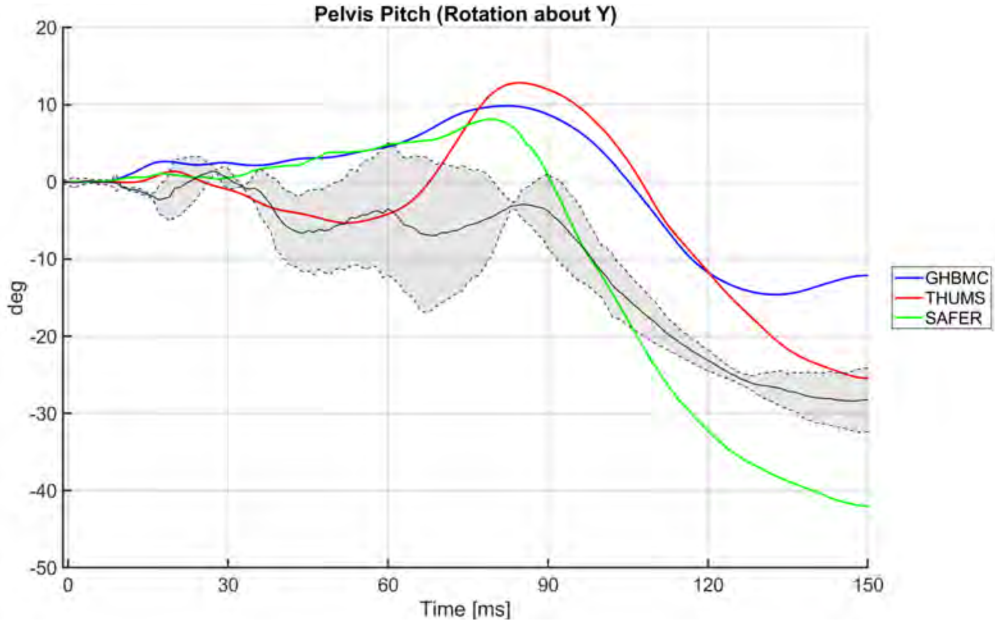

Figure A 19: Pelvis pitch

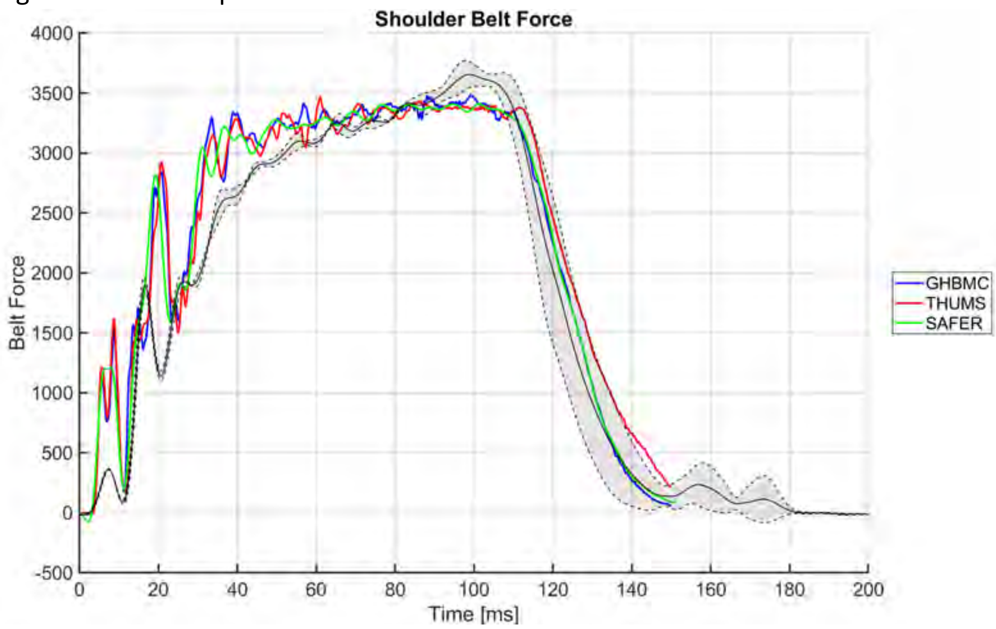

Figure A 20: Shoulder belt force

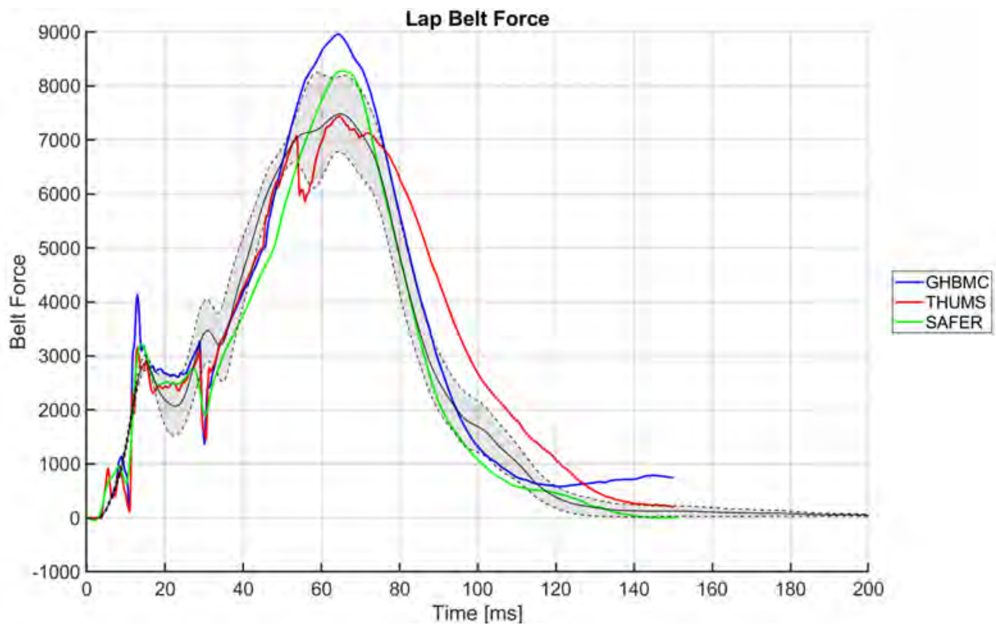

Figure A 21: Lap belt force

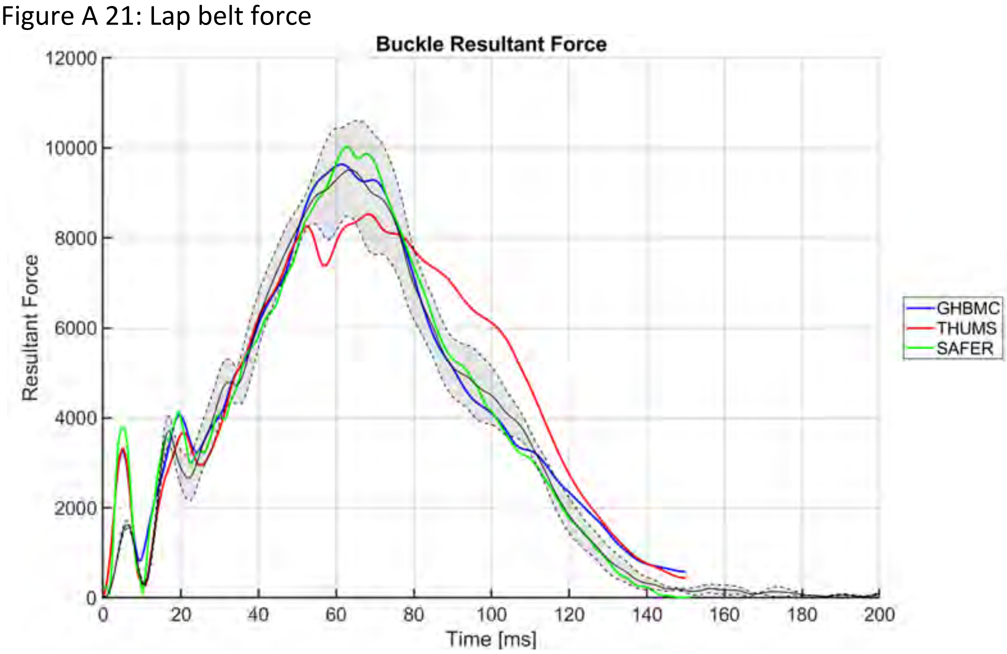

Figure A 22: Buckle resultant force

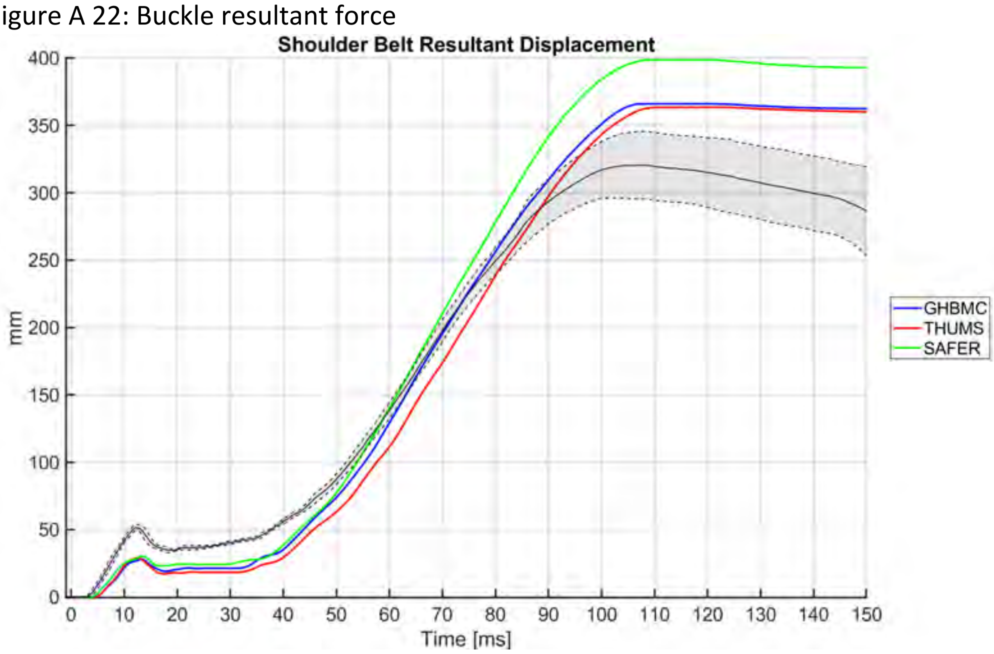

Figure A 23: Shoulder belt resultant displacement

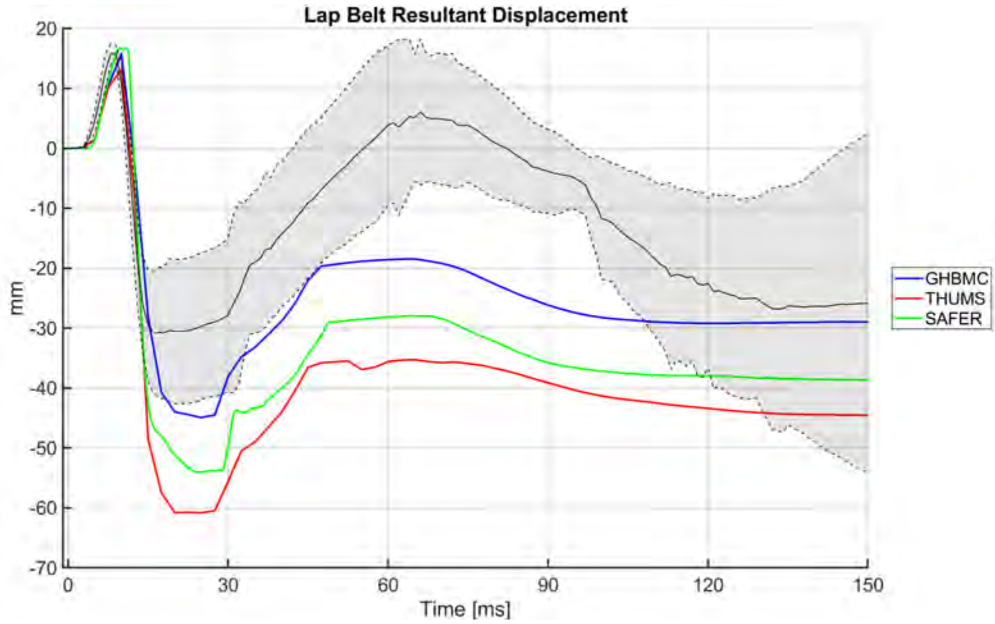

Figure A 24: Lap belt resultant displacement

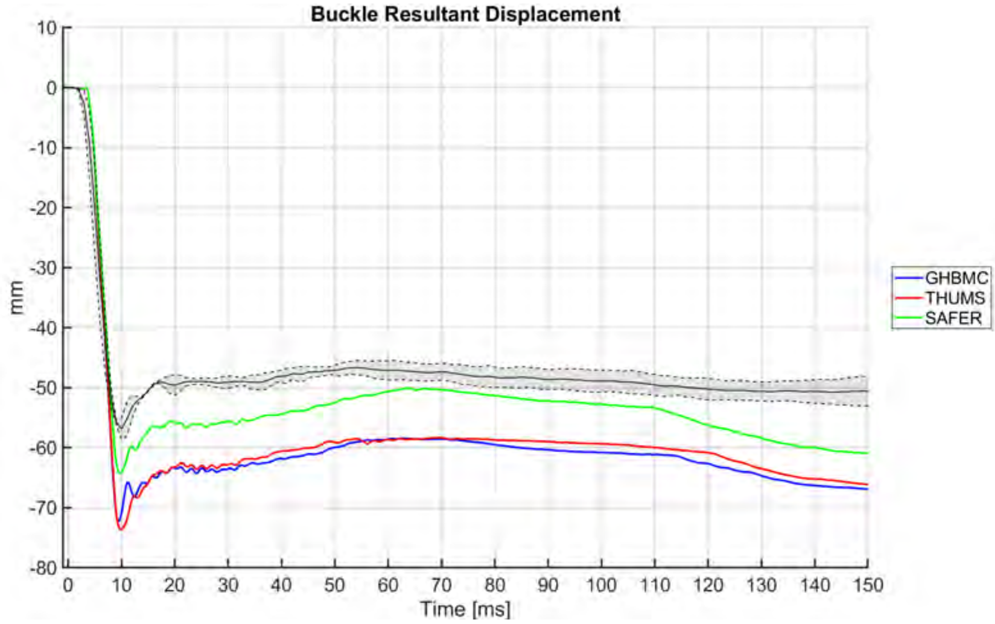

Figure A 25: Buckle resultant displacement

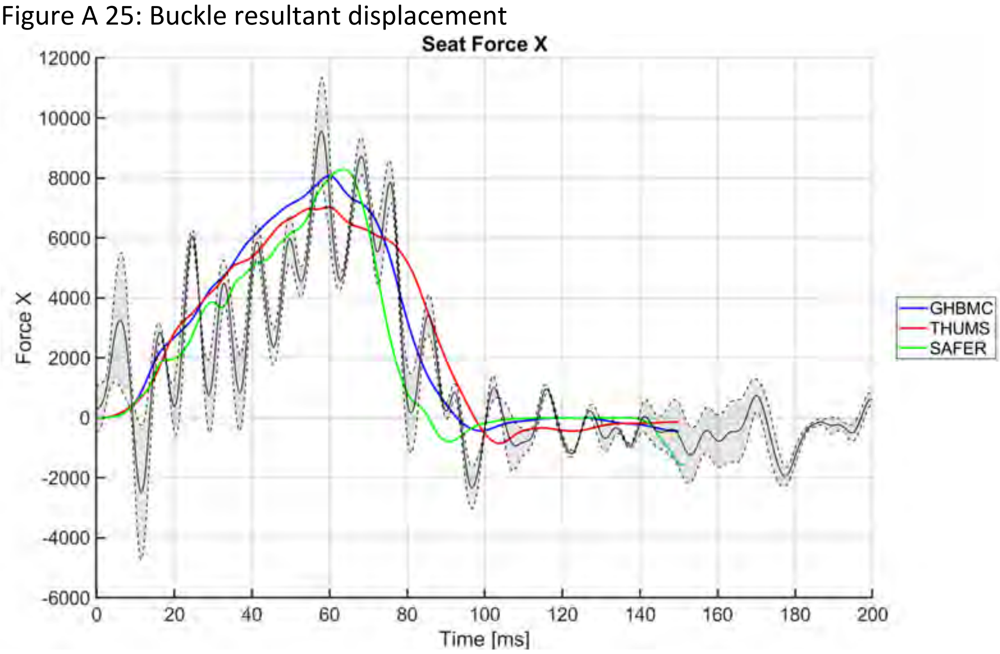

Figure A 26: Seat force X

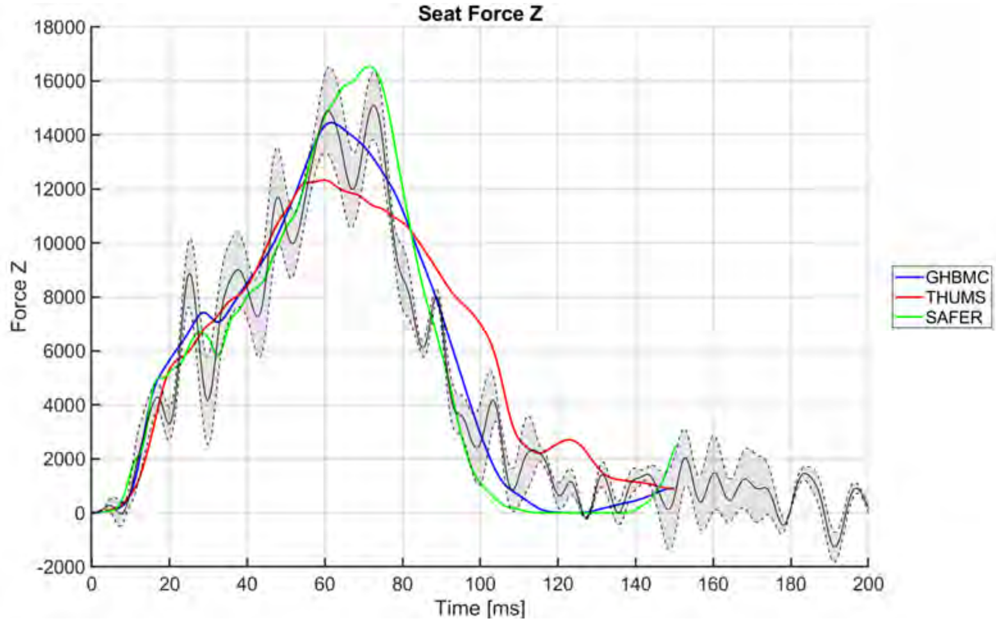

Figure A 27: Seat force Z

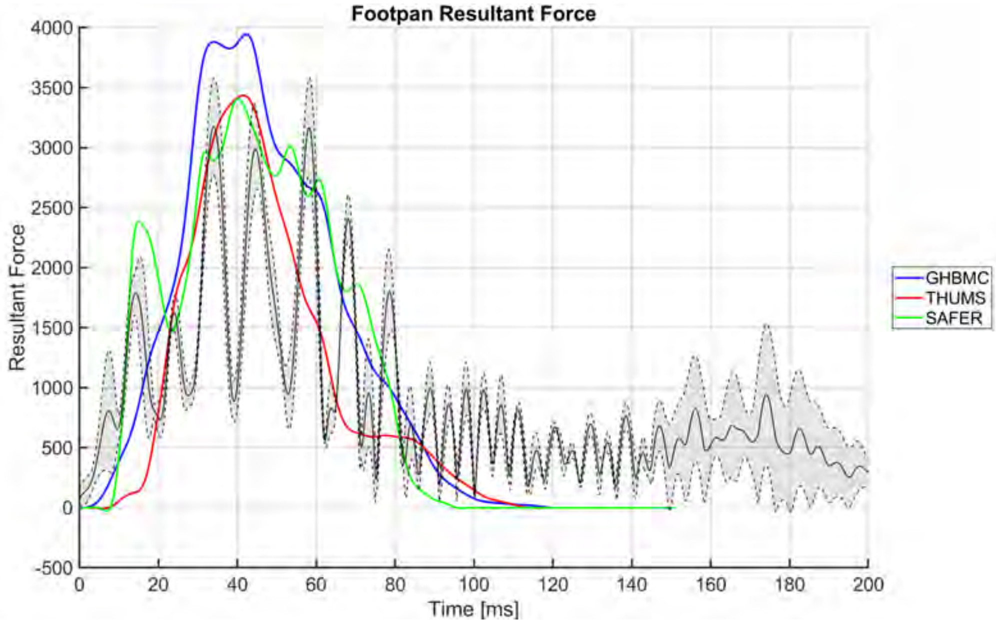

Figure A 28: Footpan resultant force

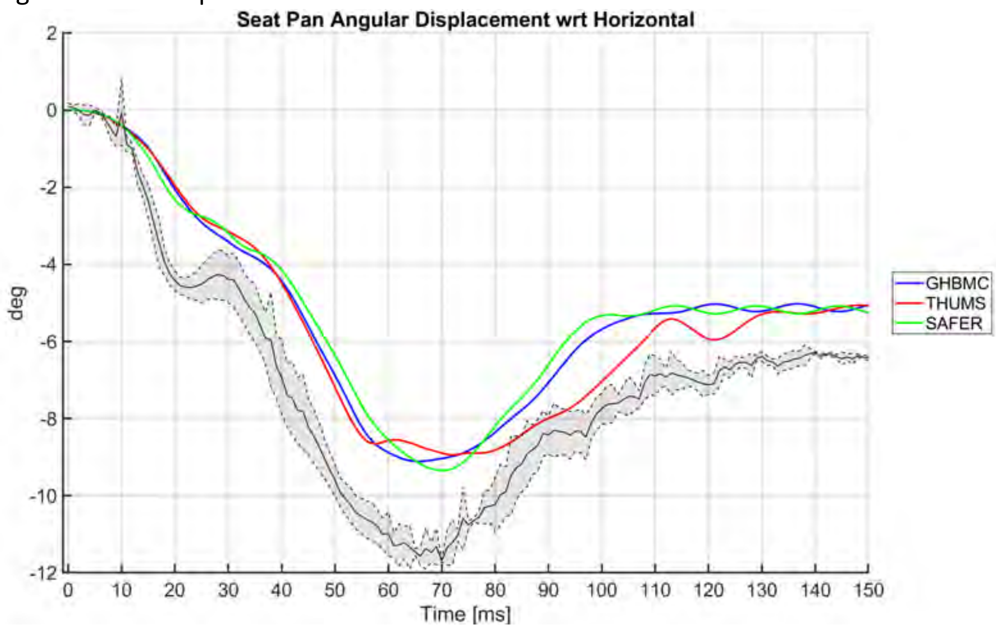

Figure A 29: Seat pan angular displacement

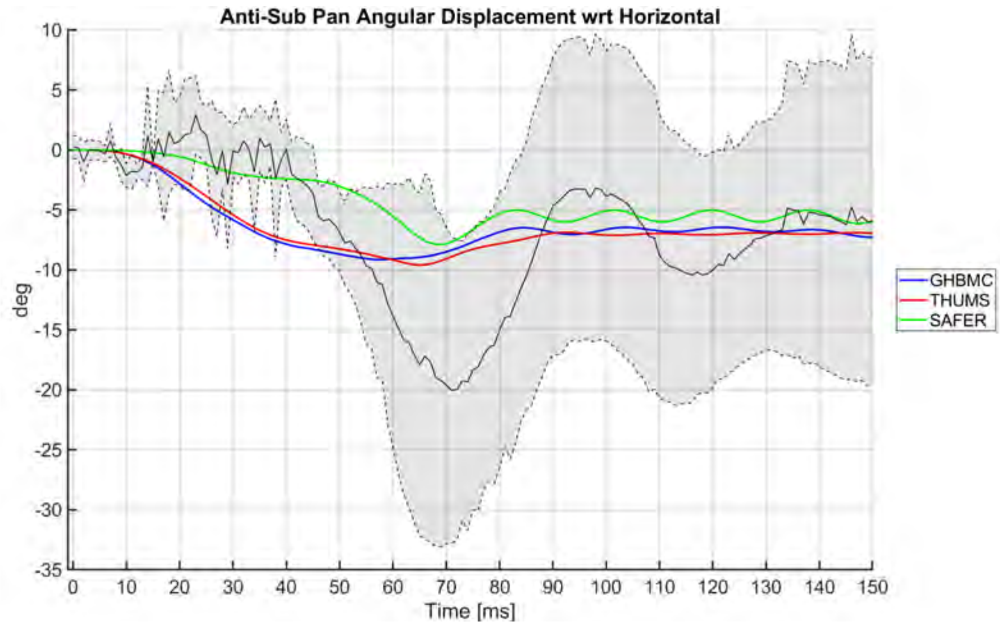

Figure A 30: Anti-sub pan angular displacement

APPENDIX B

CORA analysis

Table B I

CORA RESULTS OBTAINED FOR THE GHBMC MODEL

GHBMC	Corridor Score	Phase Score	Size Score	Progression Score	Correlation Score	Total Score
Head_disp_x	0.394	1.000	0.892	0.999	0.973	0.684
Head_disp_y	0.529	0.000	0.001	0.674	0.337	0.433
Head_disp_z	0.194	1.000	0.158	0.839	0.709	0.452
Head_rot_y	0.651	1.000	0.937	0.997	0.983	0.817
T1_disp_x	0.594	1.000	0.792	0.999	0.948	0.771
T1_disp_y	0.473	1.000	0.225	0.968	0.790	0.632
T1_disp_z	0.035	0.519	0.087	0.805	0.554	0.295
T8_disp_x	0.732	1.000	0.828	0.998	0.956	0.844
T8_disp_y	0.909	1.000	0.757	0.975	0.926	0.918
T8_disp_z	0.082	1.000	0.630	0.977	0.896	0.489
T11_disp_x	0.804	1.000	0.963	0.996	0.989	0.896
T11_disp_z	0.291	0.000	0.129	0.797	0.431	0.361
L1_disp_x	0.220	0.963	0.816	0.996	0.943	0.581
L1_disp_z	0.375	1.000	0.991	0.958	0.977	0.676
L3_disp_x	0.924	1.000	0.787	0.999	0.946	0.935
L3_disp_z	0.816	1.000	0.844	0.964	0.943	0.879
Pelvis_disp_x	0.551	1.000	0.899	0.998	0.974	0.763
Pelvis_disp_z	0.527	0.000	0.103	0.796	0.424	0.475
Pelvis_rot_y	0.267	1.000	0.306	0.814	0.734	0.500
Seatpan_pitch	0.104	1.000	0.598	0.998	0.899	0.501
Antisubpan_pitch	0.878	0.296	0.538	0.935	0.676	0.777
Shoulder_belt_resultant	0.295	1.000	0.793	0.998	0.947	0.621
Lap_belt_resultant	0.632	1.000	0.433	0.929	0.823	0.727
Buckle_resultant	0.047	1.000	0.628	1.000	0.907	0.477
Seat_force_x	0.437	0.933	0.813	0.956	0.915	0.676
Seat_force_z	0.613	1.000	0.911	0.993	0.974	0.794
Footpan_resultant	0.165	1.000	0.518	0.937	0.848	0.507
Shoulder_belt_force	0.435	1.000	0.903	0.995	0.973	0.704
Lap_belt_force	0.606	1.000	0.825	0.996	0.954	0.780
Buckle_force_resultant	0.678	1.000	0.980	0.998	0.994	0.836

Table B II
CORA RESULTS OBTAINED FOR THE THUMS MODEL

THUMSv6	Corridor Score	Phase Score	Size Score	Progression Score	Correlation Score	Total Score
Head_disp_x	0.441	1.000	0.991	1.000	0.998	0.719
Head_disp_y	0.673	1.000	0.086	0.975	0.759	0.716
Head_disp_z	0.224	1.000	0.208	0.809	0.707	0.465
Head_rot_y	0.822	1.000	0.941	0.999	0.984	0.903
T1_disp_x	0.651	1.000	0.784	0.999	0.946	0.798
T1_disp_y	0.567	1.000	0.946	0.976	0.975	0.771
T1_disp_z	0.074	1.000	0.196	0.942	0.770	0.422
T8_disp_x	0.450	1.000	0.711	0.998	0.927	0.688
T8_disp_y	0.959	1.000	0.903	0.880	0.916	0.937
T8_disp_z	0.107	1.000	0.653	0.986	0.906	0.507
T11_disp_x	0.432	1.000	0.811	0.995	0.951	0.691
T11_disp_z	0.309	0.000	0.191	0.604	0.350	0.329
L1_disp_x	0.186	0.741	0.930	0.994	0.915	0.550
L1_disp_z	0.400	1.000	0.954	0.971	0.974	0.687
L3_disp_x	0.900	0.667	0.948	0.998	0.903	0.901
L3_disp_z	0.830	1.000	0.881	0.976	0.958	0.894
Pelvis_disp_x	0.108	0.593	0.709	0.990	0.820	0.464
Pelvis_disp_z	0.470	0.000	0.778	0.701	0.545	0.508
Pelvis_rot_y	0.471	1.000	0.580	0.866	0.828	0.650
Seatpan_pitch	0.181	1.000	0.655	0.997	0.912	0.547
Antisubpan_pitch	0.888	0.593	0.580	0.938	0.762	0.825
Shoulder_belt_resultant	0.223	1.000	0.833	0.997	0.956	0.590
Lap_belt_resultant	0.288	1.000	0.188	0.913	0.754	0.521
Buckle_resultant	0.047	1.000	0.644	1.000	0.911	0.479
Seat_force_x	0.433	0.985	0.874	0.949	0.939	0.686
Seat_force_z	0.528	0.830	0.950	0.986	0.938	0.733
Footpan_resultant	0.223	1.000	0.855	0.916	0.922	0.573
Shoulder_belt_force	0.382	1.000	0.894	0.994	0.971	0.676
Lap_belt_force	0.495	0.770	0.911	0.995	0.918	0.706
Buckle_force_resultant	0.414	0.956	0.948	0.993	0.972	0.693

Table B III
CORA RESULTS OBTAINED FOR THE SAFER MODEL

SAFER	Corridor Score	Phase Score	Size Score	Progression Score	Correlation Score	Total Score
Head_disp_x	0.306	1.000	0.887	0.999	0.971	0.639
Head_disp_y	0.492	0.000	0.153	0.561	0.319	0.406
Head_disp_z	0.554	1.000	0.830	0.916	0.916	0.735
Head_rot_y	0.757	1.000	0.997	0.999	0.999	0.878
T1_disp_x	0.640	1.000	0.789	1.000	0.947	0.794
T1_disp_y	0.481	1.000	0.385	0.990	0.841	0.661
T1_disp_z	0.291	1.000	0.355	0.961	0.819	0.555
T8_disp_x	0.628	1.000	0.775	0.999	0.943	0.786
T8_disp_y	0.852	0.148	0.748	0.592	0.520	0.686
T8_disp_z	0.538	1.000	0.948	0.994	0.984	0.761
T11_disp_x	0.891	1.000	0.974	0.999	0.993	0.942
T11_disp_z	0.339	0.000	0.036	0.500	0.259	0.299
L1_disp_x	0.168	1.000	0.749	0.999	0.937	0.553
L1_disp_z	0.465	1.000	0.655	0.994	0.911	0.688
L3_disp_x	0.910	0.889	0.689	0.999	0.894	0.902
L3_disp_z	0.856	1.000	0.595	0.996	0.897	0.876
Pelvis_disp_x	0.378	1.000	0.982	0.988	0.989	0.683
Pelvis_disp_z	0.700	1.000	0.506	0.908	0.831	0.765
Pelvis_rot_y	0.435	1.000	0.524	0.965	0.864	0.649
Seatpan_pitch	0.084	1.000	0.573	0.998	0.892	0.488
Antisubpan_pitch	0.964	1.000	0.295	0.953	0.800	0.882
Shoulder_belt_resultant	0.134	1.000	0.668	0.998	0.916	0.525
Lap_belt_resultant	0.360	1.000	0.246	0.917	0.770	0.565
Buckle_resultant	0.070	1.000	0.808	0.999	0.952	0.511
Seat_force_x	0.434	0.726	0.975	0.958	0.904	0.669
Seat_force_z	0.563	1.000	0.856	0.991	0.959	0.761
Footpan_resultant	0.198	0.978	0.602	0.938	0.864	0.531
Shoulder_belt_force	0.454	1.000	0.910	0.996	0.976	0.715
Lap_belt_force	0.761	1.000	0.960	0.996	0.988	0.875
Buckle_force_resultant	0.796	1.000	0.977	0.998	0.993	0.895